Permanganate oxidation of polycyclic aromatic compounds (PAHs and polar PACs): column experiments with DNAPL at residual saturation

Clotilde Johansson, Philippe Bataillard, Coralie Biache, Catherine Lorgeoux, Stéfan Colombano, Antoine Joubert, Christian Défarge, Pierre Faure

Permanganate oxidation of polycyclic aromatic compounds (PAHs and polar PACs): column experiments with DNAPL at residual saturation

Clotilde Johansson [1,2,3,4], Philippe Bataillard [2], Coralie Biache [1], Catherine Lorgeoux [3], Stéfan Colombano [2], Antoine Joubert [4], Christian Défarge [5,6], Pierre Faure[1]*

[1] Université de Lorraine, CNRS, LIEC, F-54000 Nancy, France
[2] Bureau de Recherches Géologiques et Minières (BRGM), 45060 Orléans, France
[3] GeoRessources, CREGU, CNRS, Université de Lorraine, F-54000 Nancy, France
[4] SERPOL, 2 Chemin du Génie, BP 80, 69633 Vénissieux, France
[5] Institut des Sciences de la Terre d'Orléans, UMR 7327 Université d'Orléans-CNRS/INSU-BRGM, Polytech'Orléans, 45072 Orléans Cedex 2, France
[6] CETRAHE, Université d'Orléans, Polytech'Orléans, 45072 Orléans Cedex 2, France
*Pierre Faure : pierre.faure@univ-lorraine.fr

Abstract

Permanganate is an oxidant usually applied for in situ soil remediation due to its persistence underground. It has already shown great efficiency for dense nonaqueous phase liquid (DNAPL) degradation under batch experiment conditions. In the present study, experimental permanganate oxidation of a DNAPL — coal tar — sampled in the groundwater of a former coking plant was carried out in a glass bead column. Several glass bead columns were spiked with coal tar using the drainage-imbibition method to mimic on-site pollution spread at residual saturation as best as possible. The leaching of organic pollutants was monitored as the columns were flushed by successive sequences: successive injections of hot water, permanganate solution for oxidation, and ambient temperature water, completed by two injections of a tracer before and after oxidation. Sixteen conventional US-EPA PAHs and selected polar PACs were analyzed in the DNAPL remaining in the columns at the end of the experiment and in the particles collected at several steps of the flushing sequences. Permanganate oxidation of the pollutants was rapidly limited by interfacial aging of the DNAPL drops. Moreover, at the applied flow rate chosen to be representative of in situ injections and groundwater velocities, the reaction time was not sufficient to reach high degradation yields but induced the formation and the leaching of oxygenated PACs.

Keywords: Soil and groundwater remediation; O-PAC ketones; Potassium permanganate; Dense nonaqueous phase liquid; Column flow-through experiments

Highlights

- KMnO4 oxidation of PAHs and polar PACs from a DNAPL was monitored.
- The KMnO4 reaction was more limited as the DNAPL-water interface evolved.
- DNAPL oxidation by KMnO4 formed many ketones that leached from the column.

Introduction

The iron and steel industries developed in many countries in the past century, and the ensuing coke production generated coal tar pollution. As the health and environmental risks related to this by-product were not known at that time, it was usual to store it in tanks that were sometimes not totally impermeable and eventually dispose of it on internal dumps. As a viscous liquid, tar sank through the waste down to the soil and formed pools of dense or light nonaqueous phase liquids (DNAPL-LNAPL) in subsoils and aquifers. Wastelands of former coking plants are therefore often highly impacted with coal tar spills containing hundreds of different compounds, mostly polycyclic aromatic hydrocarbons (PAHs) and/or polar polycyclic aromatic compounds (polar-PAC) containing at least one heteroatom (nitrogen, sulfur or oxygen) (Brown et al. 2006; Birak and Miller 2009).

DNAPL pools have shown great stability and persistence over time, acting as active contaminant sources for groundwater and spreading plumes for decades. Many studies dealing with the leaching of PACs through column experiments have been conducted. Two important conclusions have been drawn: (i) low–molecular-weight PAHs are preferentially dissolved in the water phase (Broholm et al. 1999; Benhabib et al. 2010; Boulangé et al. 2019a), whereas higher–molecular-weight PAH mobility is associated to colloidal transport (Boulangé et al. 2019a), and (ii) the proportion of polar PACs dissolved in water from the DNAPL is much higher than the equivalent proportion of PAHs (thanks to the higher polar PAC polarity and solubility) (Benhabib et al. 2010; Lundstedt et al. 2007; Schlanges et al. 2008; Boulangé et al. 2019a; Kleineidam et al. 2004).

Some remediation techniques are aimed at extracting pure NAPL (free product), whereas others, like in situ chemical oxidation (ISCO), are aimed at degrading the remaining pollutants (residual saturation). Chemical oxidation aims to transform pollutants into CO2 and water by complete mineralization or into smaller organic residues likely to be further degraded through biological processes. However, incomplete oxidation of PAHs can lead to the formation of oxygenated PACs (O-PACs) (Forsey et al. 2010; Biache et al. 2011; Guan et al. 2014; Pardo et al. 2016; Ranc et al. 2017). Some of these oxygenated by-products have shown high toxicity (Durant et al. 1996; Sverdrup et al. 2002; Xue and Warshawsky 2005; Lampi et al. 2006; Lundstedt et al. 2007; Andersson and Achten 2015), in some cases even higher than the parent PAHs. Ketones are particularly strong mutagenic agents (Pedersen et al. 2004). Combined with their higher solubility in water compared to PAHs, their formation during oxidation processes during soil remediation is of great concern.

Numerous studies, mainly batch experiment ones, have demonstrated the efficiency of chemical oxidants to degrade PACs in contaminated soils (Forsey et al. 2010; Lemaire et al. 2013a; Trellu et al. 2016; Usman et al. 2016; Ranc et al. 2017; Johansson et al. 2020). A few works have addressed oxidation under flow-through conditions with column experiments. They focused on the use of activated persulfate or hydrogen peroxide (Fenton or Fenton-like) alone (Usman et al. 2013; Lemaire et al. 2013b; Pardo et al. 2016) or combined with extraction methods: addition of a chelating agent — sodium pyrophosphate (Venny and Ng 2012) or cyclodextrin (Lemaire et al. 2013b). These studies did not focus on the formation of polar PACs during these oxidation reactions. Moreover, the spiking methods implied solvent-dissolved standard PAHs, or pollutants extracted from contaminated soil and homogeneously blended in a reference uncontaminated sand or soil before column packing. The spiking method chosen in our study is aimed at mimicking field conditions, especially with nonhomogeneous DNAPL spreading, using a drainage-imbibition experimental setup.

Permanganate oxidation in porous media under flowthrough conditions is more frequently described on chlorinated solvent-DNAPL (Conrad et al. 2002; Chong and Mayer 2017; Matta and Chiron 2018). After the reaction, permanganate produces MnO2 precipitates that may agglomerate and form larger particles likely to clog the pores of the medium (Sirguey et al. 2008).

In a recent study, the efficiencies of several oxidants (permanganate, heat-activated persulfate, Fenton-like reactions with magnetite as a catalyst, ferrates) to oxidize PAHs and polar PACs from a sand spiked with coal tar DNAPL were compared in batch experiments (Johansson et al. 2020). Permanganate led to high degradation yields for PAHs, polar PACs, and total DNAPL mass, but also to O-PAC ketone formation.

Batch experiments (thanks to homogeneous spiking of the solid medium and continuous stirring) offer an ideal and homogeneous contact between oxidants and pollutants. On the contrary, oxidations carried out under flow conditions (columns) often face problems of preferential pathways, limited contact time, and heterogeneous behavior (depending on the settings) that are more representative of ISCO field application. Lower degradation rates and efficiencies are expected with column experiments and therefore potentially higher concentrations of residual by-products (especially O-PACs).

To the best of our knowledge, permanganate oxidation of DNAPL-spiked (PAH- and PAC-spiked) matrices had never been applied to column experiments yet, whereas permanganate oxidation of PAH-contaminated matrices has already shown high efficiency in batch experiments (Ranc et al. 2017; Boulangé et al. 2019b; Lemaire et al. 2019; Johansson et al. 2020). Moreover, the formation of metal-oxide precipitates and oxygenated PAC intermediates as by-products is expected to have an impact on the porous medium and the water leachate quality during oxidation.

This work is aimed at studying the impact of permanganate on PAHs and polar PACs from coal tar DNAPL and spiked in columns in a similar way as they would be distributed in a contaminated aquifer. Special attention was paid to (i) the flow path and porosity and (ii) pollutant and by-product transfer that could alter the quality of the water leachates.

This study does not focus on the quantitative efficiency of oxidation but on its qualitative evolution to determine if hazardous by-products of oxidation may leach from the system.

Materials and methods

Chemicals

The solvents used for organic extraction and analysis were dichloromethane DCM (puriss ACS reagent ISO (GC) 99.9% from Sigma Aldrich), acetone (HPLC grade — BioSolve), and n-hexane (HPLC grade — BioSolve). Potassium bromide (KBr 99%+, Alfa Aesar) and magnesium sulfate ($MgSO_4$, 99% Extra Pure, SLR, Dried, Fisher Chemical) were used to perform tracer experiments and to stabilize the conductivity of the deionized (DI) water to 1,500 µs/cm, respectively. DI water was produced with an Elix® Essential water purification system connected to a Milli-Q® Gradient A10 from Merck.

Matrices Origin of the dense nonaqueous phase liquid (DNAPL) and sampling site characteristics The DNAPL used in this study was sampled at 3–4-m depth in the aquifer of a former coking plant (Lorraine, France). Its molecular composition is detailed in our previous work (Johansson et al. 2020). It is dominated by naphthalene, methyl- and ethyl-naphthalenes, acenaphthene, fluorene, phenanthrene, and dibenzofuran. Its elemental composition was C: 84.1 wt%, H: 5.8 wt%, N: 0.3 wt%, O : 5.3 wt%, and S: 4.1 wt% (determined by catalytic combustion in an Elementar Vario Micro Cube by the Laboratory of Physical Measurements of Montpellier University — France). The site is located in eastern France. It is located on an alluvial groundwater made up of coarse sands with less permeable layers (fine to silty sand). The hydrogeological characteristics of the groundwater are as follows: hydraulic conductivi ty : 3 .3 × 10^{-4} m/s, transmissivity: 1.37 × 10^{-3} m^2 /s, storage coefficient: 5.27 × 10^{-3} , porosity: 0.35.

Porous medium

The column experiments were carried out on 1 ± 0.1-mm diameter glass beads (Sablières Palvadeau les Douemes), chosen to be in the range of the mean textural (sandy) characteristics of the site. Oxidant and water solution The DI water solutions used to flush the columns were (i) spiked with magnesium sulfate to reach a conductivity of 1,500 µS/cm (concentration of 1.59 g/L), corresponding to the medium value measured in the underground water of the DNAPL sampling site, and (ii) sonicated (Elmasonic S 60H from Elma) for at least 30 min to limit the formation of gaseous bubbles in the porous medium, because bubbles can limit porosity and disturb the flows. These solutions are referred to as "WS" throughout the paper. Potassium permanganate ($KMnO_4$ 99+%, Acros Organics) was dissolved in the WS at different concentrations for the injections.

Column experiments

Glass beads (336.9 ± 3.0 g) were packed in borosilicate glass columns (VERAL equipment, column 4.9-cm internal diameter, 9.6-cm high, plus two cones with sintered glass filters (4– 5-mm thick) of variable sizes and volumes (between 30 and 50 mL)) held vertically. Two different columns were prepared in duplicate: (i) a control one and (ii) a permanganate-oxidized one. The control experiments were stopped after the hot water flushing (HWF) and tracer experiments (BC1), whereas the oxidized columns were additionally flushed with permanganate (OXI), rinsed with water (FWF), and underwent a second tracer experiment (BC2). Solutions and reactants were injected in an ascending flow. Several steps were successively carried out:

– Sequence 1: initial spiking by drainage-imbibition
– Sequence 2: hot water flushing (HWF)
– Sequence 3: tracer experiment, breakthrough curves be- fore oxidation (BC1)
– Sequence 4: oxidation (OXI)
– Sequence 5: final water flushing (FWF)
– Sequence 6: tracer experiment, breakthrough curves after oxidation (BC2)

Sequence 1 — initial spiking by drainage-imbibition

In order to mimic on-site pollution spread as best as possible, the drainage-imbibition method was used (Colombano et al. 2020).

Water saturation of the porous medium (Figure S1a) A 250-mL burette was connected to the top of the column. The columns were first filled with slowly pumped WS (< 50 mL/h) in an ascending flow until water was visible inside the water burette (lowest graduation).

Drainage (DNAPL injection) (Figure S1b) The systems were closed by pinching the tube underneath the column, and a second 250-mL burette was connected to the lower part of the column and filled with DNAPL up to the equilibrium level, calculated from the waterfront using the following formula: $h_{DNAPL} = h_{water} \times \rho_{water}/\rho_{DNAPL}$, with h the height (mm) and ρ the fluid density (g/L). DNAPL density was measured at 1.09 g/L with a densimeter (Philippe et al. 2020). Then, the tube was opened, and the system was left to equilibrate overnight.

The DNAPL burette was raised by 1.5- to 3-cm steps spaced out by 1–2-h stabilization steps (or overnight), until the DNAPL had filled the whole porous medium and the upper cone and was visible in the water burette (total time: 7 days). The system was maintained in darkness for 2 days to reach equilibrium. Levels and volumes were measured after each stabilization time.

Imbibition (water injection) (Figure S1c) The opposite movement was applied, the DNAPL burette was lowered similarly by 1.5- to 3-cm steps until no DNAPL was visible in the lower cone of the column (total time: 7 days). The water replaced DNAPL in the column, except for residual DNAPL remaining in the porous medium.

The tube under the column was pinched again, and the burettes were disconnected from the column. The upper cone was closed with a plug, and the columns were left in darkness at room temperature for 2 days before switching to the flushing setup (Figure S1c).

Volumes were measured throughout the experiment, and the glassware masses were determined to calculate (i) the mass difference between the DNAPL added to the system and the DNAPL extracted after drainage-imbibition and (ii) the residual saturation of the DNAPL in the column.

Sequence 2: hot water flushing (HWF) — pore volume (Pv) =0 to Pv=55

In DNAPL-polluted soil, thermal pumping is generally first used to remove the maximum quantity of pure DNAPL phases from the aquifer before applying other complementary treatments. In our experiment, this step was performed to mimic a heat-enhanced pumping treatment and to reach equilibrium with water flushing prior to oxidation.

WS was heated at 70 °C in a water bath (Polystat 36 immersion circulator from Fisher Scientific). Tubes were connected from this stock solution to the lower part of the columns by a pump that injected the solution in an ascending flow of 100 mL/h (Figure S1c).

The flow rate of 100 mL/h was chosen to be similar to the hydrogeological characteristics of the site (see the "Origin of the dense nonaqueous phase liquid (DNAPL) and sampling site characteristics" section) and correspond to the measured flow. Corresponding to a hydraulic velocity of 3.5 10−5 m/s, the flow was a compromise between laboratory limitations and field conditions (see the "Origin of the dense nonaqueous phase liquid (DNAPL) and sampling site characteristics" section).

Higher flow rates were applied twice during the hot water flushing step to rapidly raise the temperature inside the porous medium (Fig. 1). Two columns underwent injections at 1446 mL/h as the highest flow rate (Col-Ctrl-1, Col-Ctrl-2), and two columns were flushed at 494 mL/h during the high flow steps (Col-Mn-1, Col-Mn-2). This choice was made to study the impact of the flow rate on the remobilization of pollutants.

The columns were wrapped with isolating cover foil to maintain the heat as long as possible. The WS was injected at 70 °C, and temperature measured in the leachates of ColCtrl-1 and Col-Ctrl-2 rose from 25 to 43.1 °C and 48.1 °C during the 1446-mL/h flow rate periods, respectively, whereas temperature measured in the leachates of Col-Mn-1 and ColMn-2 only rose from 20 to 26 °C during the 494-mL/h flow periods, respectively. Between those two high flow times, temperature decreased slowly back to 20 °C for all the columns (measured at the collection point).

Sequence 3: tracer injection — breakthrough curves after the hot water flushing step (BC1), Pv=55 to Pv=85

For the ascending curve, KBr was dissolved in the WS (20 mg/L) and injected (19.9 Pv) at 100 mL/h in an ascending flow and at room temperature. Outlet solutions were collected in 20-mL glass flasks to monitor the evolution of the leachate at a finer scale (0.24 Pv).

With WS injection, the decrease in bromide ions in the outlet solution allowed us to determine the breakthrough curves (further 6.5 Pv). At the end of the flushing steps, the columns were closed (the tubes were pinched) and left in darkness at room temperature for 3 days. At the end of this sequence, the two control columns (Col-Ctrl-1 and Col-Ctrl2) were dismantled to extract and analyze the remaining DNAPL.

Sequence 4: oxidation (OXI) — Pv=85 to Pv=307

All injections were carried out at 100 mL/h, ascending flow, with the oxidant dissolved in the previously prepared WS (cf. the "Column experiments" section).

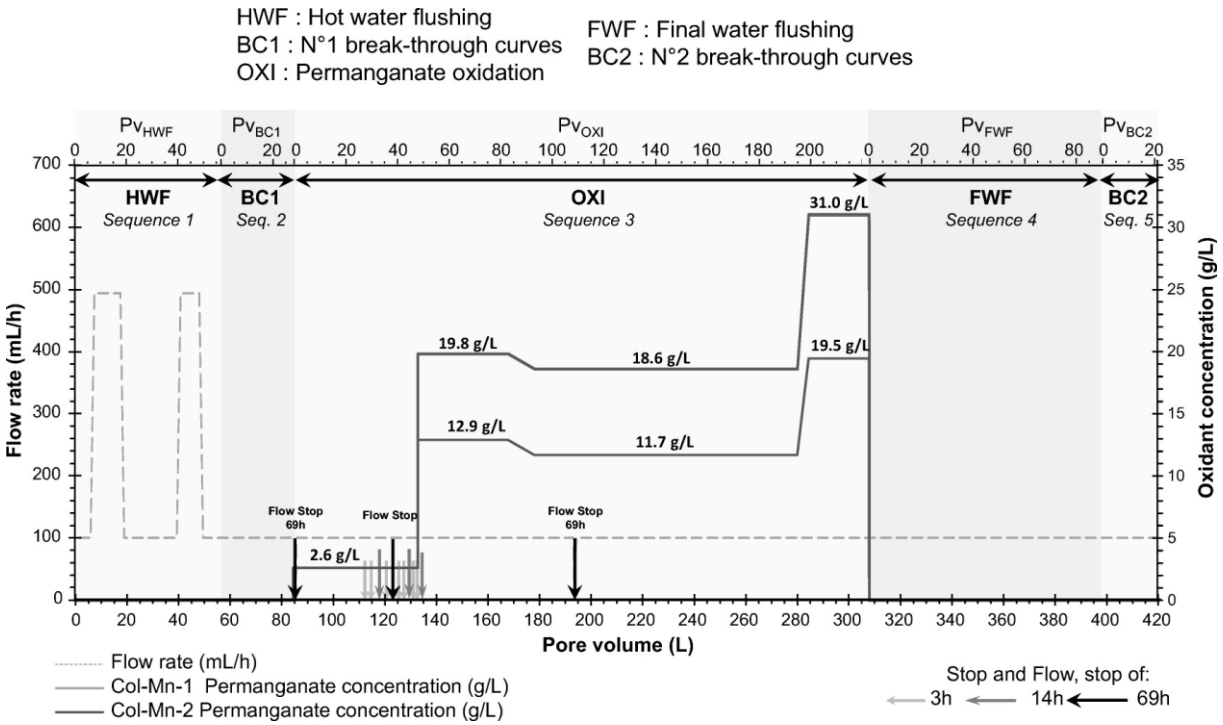

Fig.1: Injection protocol for permanganate-treated columns — 5 steps: hot water flushing (HWF); n°1 break-through curves (BC1); oxidation (OXI); final water flushing (FWF); and n°2 break-through curves (BC2). The volumes eluted from the columns are given as total pore volumes (bottom X-axis) and as the pore volume (Pv) of each step (top X-axis)

Oxidation procedure Permanganate is stable for days in aqueous solution and even persistent for months when used in soils (Huling and Pivetz 2006; Rancetal.2017), but our objective was to study the time-limited contact in flow-through conditions. Therefore, oxidations were applied for 2 weeks. As permanganate is likely to generate high a mounts of oxide precipitates that may clog porous media, a two-step oxidative injection was performed to test the behavior of the oxidant, starting with the lowest concentration (2,6 g/L for the two columns) and then the highest concentrations (up to 19.5 and 31.0 g/L for Col-Mn-1 and Col-Mn-2, respectively) (Fig. 1).

After the injection of 8.7-Pv oxidant, the solution came out of the column with similar concentrations of permanganate in the injected solution and the leachates, as revealed by UV absorbance measurements (not shown). Knowing the persistent character of PACs, “stop-and-flow” sequences were applied, with stop times of 3h, 14h, and 69h to give the oxidant time to react with the pollutants, before resuming continuous flushing (Fig. 1).

The oxidant content was provided in a deficient amount to check for the formation of by-products and whether the leachates were impacted; that is why oxidation was stopped after the injection of 0.35 stoichiometric oxidant demand (SOD). A total of 222-Pv oxidant was injected through each column.

Oxidant dose It was calculated similarly to previous experiments (Johansson et al. 2020), using the stoichiometric molar ratio (SMR) based on elemental analysis of DNAPL, as proposed by Ranc et al. (2016). The total mass of residual DNAPL was considered as the extractable organic matter (EOM) and was used to calculate the SOD.

In general, potassium permanganate concentrations applied on site range from 2 to 5 g/L (Simonnot and Croze 2012). Therefore, permanganate was injected at 2.6 g/L in each column for the first injection step. Then, the concentrations increased according to requirements: Col-Mn-1 was treated with

solutions concentrated at 2.6 g/L, 12.9 g/L, 11.7 g/L, and 19.5 g/L, and Col-Mn-2 was treated with solutions concentrated at 2.6 g/L, 19.8 g/L, 18.6 g/L, and 31.0 g/L (Fig. 1).

Sequence 5: final water flushing (FWF) — Pv=307 to Pv=397

Without any stop time, the WS was injected after the end of oxidation at room temperature (100 mL/h). This helped remove the oxidant and see how leachates were stabilizing after oxidation. Col-M n-1 and Col-Mn-2 were flushed with 85 Pv.

Sequence 6: tracer experiment — breakthrough curves after oxidant injection (BC2), Pv=397 to Pv = 420

The breakthrough curves (BC2) were measured after the final water flushing sequence following the same protocol as before oxidation (BC1 — sequence 3).

Collection of the fractions and management of the leachate samples

Outlet water samples were continuously collected during sequences 2, 4, and 5, mostly in 100-mL brown glass flasks (1.45 Pv). Only the fractions of the tracer experiment were collected in smaller volume flasks (20 mL).

All collected samples were kept at 4°C in darkness and brought back to room temperature before analysis.

Some water samples were filtrated on pre-weighed GF/F Whatman glass microfiber filters (0.7 µm) to collect particles and DNAPL blobs expelled in the water phase. To remove water, the filters were freeze-dried and weighed.

Column dismantling and extraction

At the end of the experiment, each column was dismantled as follows: the upper cone was first disconnected and placed in a beaker to collect the water and the organic phase. The glass beads were removed and placed in a beaker. Glassware and the glass beads were extracted with DCM at room temperature. Liquid-liquid separations were performed in separating funnels to remove water from the DCM extract. Then, the EOM from the column and cones was recovered in the DMC. This sample was stored in darkness at 4 °C before analysis.

Analytical methods

Global leachate parameters

Water pH, conductivity, and the redox potential (Eh) were measured in the collected samples using a WTW Multi 3420 digital meter and the corresponding pre-calibrated pH conductivity and redox probes.

The Br-ion concentration in water was analyzed after filtration at 0.45 µm (Minisart Syringe Filter NML Hydrophilic — Sartorius) with an ionic chromatography device (Thermo Dionex — ICS3000) according to the NF EN ISO 10304-1 (07/2009) standard.

Total organic and inorganic carbon (TOC-TIC)

Total organic carbon (TOC) and total inorganic carbon (TIC) measurements were carried out on the raw solutions (not filtered), whereas dissolved organic carbon (DOC) was determined after filtration of the water on a glass microfiber filter (GF/F, Whatman 0.7 µm). Measurements were carried out with a calibrated O.I. Analytical Total Organic Carbon Analyzer 1010 — Physitek.

Blank permanganate solutions were analyzed, and the results showed that the oxidant did not contribute to TOC at any concentration (< 0.1 mg/L) but induced a TIC response: TIC increased linearly along with increasing permanganate concentrations. A calibration curve was determined to correct the values. The subsequent results were corrected accordingly.

Identification and evolution of the organic fingerprint

UV measurements Absorbance was measured with a Cary 60 UV-Vis (Agilent Technologies) in a quartz cell (1-cm path length), with an absorption time of 1 s. Different wavelengths were used depending on the target: between 200 and 800 nm for a complete screening, 254 nm for aromatic structures (Touraud et al. 1998), and 525 nm for permanganate (Crimi and Siegrist 2004; Waldemer and Tratnyek 2006).

UV solution analyses were carried out as rapidly as possible (less than 15 h) after sample collection.

Absorbance measurements at 254 nm (aromatic structures) in the presence of the oxidant were not possible because the high concentration of permanganate induced absorbance at 254 nm in a non-negligible way. As a result, no 254-nm UV measurement was carried out during sequence 4 (OXI).

Fluorescence spectroscopy Fluorescence spectroscopy is used to get a rapid insight into the fingerprint (excitation-emission matrices; EEM) of fluorescent dissolved organic matter (FDOM) in water samples. Most fluorescent molecules are aromatic, so that FDOM includes natural OM (humic substances) and anthropogenic pollutants, especially PACs (Parlanti et al. 2000; Birdwell and Engel 2010; Fellman et al. 2010; Tedetti et al. 2010; Coble et al. 2014; Ferretto et al. 2014). Fluorescence spectroscopy was also used to monitor the evolution of the coal tar leachate fingerprint after air oxidation (Hanser et al. 2015). This technique can rapidly evaluate the evolution of aromaticity, which is of great interest in the experimental setup of this study.

The EEMs were acquired with an F-2500 spectrofluorometer (Hitachi), using a 10 × 10 mm mirrored quartz cell (Hellma), at a photomultiplier voltage of 400 V and with a scan speed of 1500 nm/min, over ranges of excitation and emission of 220–500 nm (λex) with 10-nm steps, and 230– 550 nm (λem) with 1-nm steps, respectively; the slit widths of the two monochromators were set at 2.5 nm. When necessary (signal extinction due to permanganate), the solutions were diluted with DI water. Scattering correction helped remove the Rayleigh and Raman interferences, and inner filter correction was applied to eliminate alterations due to primary and secondary screen effects.

Qualitative analysis of PACs by gas chromatography-mass spectrometry The extractable organic matters obtained from the column and filter extractions at the end of the experiment were analyzed in SCAN/single ion monitoring (SIM) mode by GC-MS. Sixteen PAHs (US EPA PAHs), 12 O-PACs, 5 NPACs, and 4 S-PACs were identified with a method described in a previous study (Johansson et al. 2020). The m/z values for each quantified PAC for the SIM mode are reported in Table S1.

A GC Agilent Technology 6890N was equipped with a DB-5MS column (60 m × 0.25 mm i.d. × 0.25 µm film thickness — Agilent Tech.) coupled to an Agilent 5973 inert Mass Selective Detector. One microliter of sample was injected at 300 °C in a split/splitless injector in splitless mode. The GC oven temperature was programmed from 70 °C (held 2 min) to 130 °C with a 15 °C/min ramp and then from 130 to 315 °C (held 30 min) with 4 °C/min ramp. The carrier gas was helium at a constant flow of 1.6 mL/min.

Analytical limitations Oxidant stability, reactivity, and byproduct formation were subject to several limitations.

As mentioned before, permanganate is a persistent oxidant, so that its reactivity on some components can be slow. Oxidation did not last long enough for us to reach total oxidant consumption in the porous medium, and $KMnO_4$ was still detected in outlet water leachates at the end of the experiment. Due to the high amount of residual oxidant, GC-MS quantification of water-dissolved PACs was impossible on permanganate-oxidized samples (the oxidant degraded the solid adsorbing phase

(SPE cartridges) used for PAC extraction). Therefore, PACs were not quantified in the water phase. Other analyses (TOC, fluorescence spectroscopy, etc.) were done on the leachates to monitor the evolution of the organic matter in solution.

Results

Sequence 1: DNAPL spiking by drainage-imbibition

Similar pore volumes were measured for the four glass bead columns: 71.0± 1.7 mL (Table S2).

The water solution filling the pores was considered as the wetting fluid. Drainage (DNAPL injection) ended with the coal tar (the non-wetting fluid) flowing out of the column and left a residual water content of around 30.5±3.3 %vol (volume %) in the porous medium. The reverse operation — imbibition (water solution injection) — resulted in 8.8±0.2 % vol Pv occupied by entrapped DNAPL, according to the saturation curves (Figure S2).

The total DNAPL remaining in the whole system after imbibition was measured as the mass difference between the total DNAPL injected in the column and the total DNAPL collected from the system after imbibition. The remaining DNAPL mass showed irregular results (from 20.2 to 42.6 g) among replicates (Table S2).

Sequence 2: hot water flushing (HWF)

pH, conductivity, and evolution of the redox potential during hot water flushing The pH values in the outlet leachates were slightly basic and quite constant, ca. 9.1. During the two hot water flushing steps (flow injection increased from 7.3 to 17.5 Pv_{HWF} and from 40.7 to 48 Pv_{HWF} at 1,446 mL/h), the pH decreased slowly to 8.8. No change was observed at the higher flow rate.

The conductivity of the incoming water (WS) was set at 1500 µS/cm with $MgSO_4$ addition. The initial water leachate conductivity was 1,578 ± 11 µS/cm and decreased during 4.4 PvHWF before reaching equilibrium around 1,506 ± 8 µS/cm. Neither of the hot water injections at higher rates changed the conductivity.

Those two parameters (pH and conductivity) had slightly higher values in the first leachates, probably due to soluble organic and inorganic compounds that were progressively flushed out from the raw DNAPL, as shown by TOC and TIC evolution (Fig. 2a and b).

The redox potential was stable throughout hot water flushing, even during hot water injection, with values equal to 318 ± 26 mV.

Total organic carbon (TOC) and total inorganic carbon (TIC) Outlet water leachates were collected and analyzed to monitor the evolution of carbon mobilization throughout the experiment (Fig. 2a and b).

The TOC and the TIC concentrations of the first outlet leachate samples, corresponding to water in contact with the DNAPL during the drainage-imbibition sequence (two drainage-imbibition weeks and three stagnant days), were 33.4 ± 0.9 mg/L and 15.1 ± 0.9 mg/L, respectively. Those concentrations decreased with the continuous hot water flushing (sequence 2) to reach equilibrium at 8.6 ± 1.7 mg/L and 1.3 ± 0.2 mg/L for TOC and TIC, respectively. During the higher flow rate flushing, TOC increased slightly in the outflowing water (ranging from 1.5 to 5 mg/L).

UV measurements and fluorescence spectroscopy The overall absorbance at 254 nm (Fig. 2c) decreased from 1.4 ± 0.1 (collection of the first water sample) to 0.91 ± 0.05 cm−1 (end of hot water flushing). An increase was observed following the two high flow rate injections during sequence 2 (HWF). Absorbance dropped quickly back to lower values when the flow decreased to 100 mL/h.

The SUVA aromaticity index (UV absorbance 254 nm/ dissolved organic carbon (DOC)) (Wehrer and Totsche 2005; Jeanneau et al. 2007; He et al. 2010) of organic compounds in the outlet water leachates (Fig. 2d) increased sharply following the two high flow rate injections, with a stronger increase at the

most intense flow rate (1,446 mL/h) compared to the medium one (494 mL/h). For the 100 mL/h flow rate, the SUVA index also increased from 0.042 ± 0.001 for the first sample to 0.10 ± 0.02 after 57 Pv.

The fluorescence EEMs obtained under sequence 2 (HWF leachates) showed similar fingerprints throughout the whole sequence, without any visible difference during the higher flow rate injections (Figure S3). A major peak was measured in the [λEx = 260–280 nm; λEm= 320–340 nm] region, and another peak in the [λEx = 220–230 nm; λEm= 320–340 nm] region.

Breakthrough curves were measured at a constant flow rate (100 mL/h). The bromide concentrations evolved in the same way in the 4 replicates (Col-Crtl-1 and Col-Crtl-2 and Col- Mn-1 and Col-Mn-2) (Fig. 3a), with rapid ionic saturation of the porous medium (over 2–3 pore volumes, from Pv_{BC1} =1.4 to Pv_{BC1} = 4.0), and slightly longer desaturation (over 3.5–5 pore volumes, from Pv_{BC1} =21.1toPv BC1 =25.5).

The water residence time (t_w) was calculated using:

t_w (h) = pore volume (mL)/flow rate (mL/h)

For all column replicates, t_w = 0.70 ± 0.02 h.

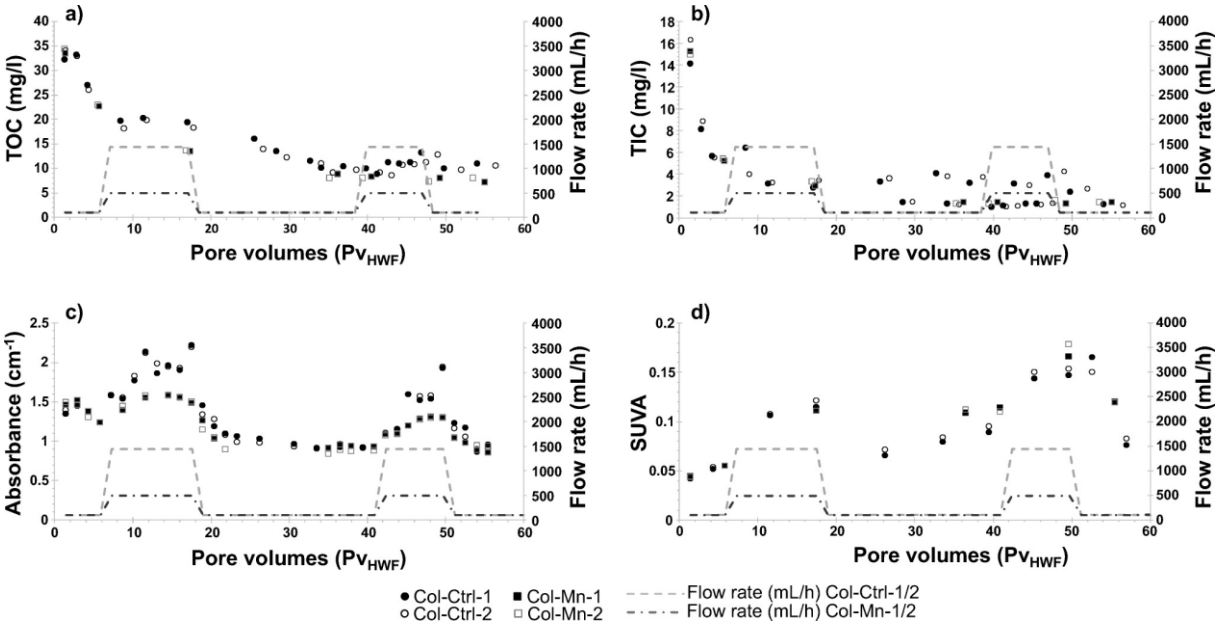

Fig. 2: Analyses of leachates from sequence 2 (hot water flushing) of the four columns: a total organic carbon (TOC) and b total inorganic carbon concentrations (TIC); c UV absorbance at 254 nm; d SUVA index (UV absorbance at 254 nm/dissolved organic carbon concentration)

The average residence time of the tracer in the porous medium (t_m) was given at the inflection point of the increasing curve (bromide = f(time)). It was measured in the replicates between 1.32 h (79 min) and 1.55 h (93 min).

The fluid velocity (v) in the pores was calculated using v = h / t_m ,with h the column height (m) and t_m in seconds. The tracer flew through the porous medium at a pore velocity of [1.72 – 2.02].10^{-5} m/s.

The absorbance at 254 nm of the outlet solution was constant at 0.78 ± 0.08 cm^{-1} during the breakthrough curve measurements (sequence 3).

Sequence 4: oxidation (OXI)

Evolution of the leachate physicochemical parameters The pH varied little in the outlet water leachates during oxidation: from 8.8 at the beginning of permanganate injection at 2.6 g/L (end of sequence 3) to 7.94 after 12 Pv_{OXI}. The pH of Col-Mn-1 rose to 8.3 and 8.7 for the highest permanganate

concentrations (11.7 g/L and 19.5 g/L, respectively) and rose to 8.8 in Col-Mn-2 for a permanganate concentration of 19.8 g/L.

Conductivity evolved rapidly: 1.5 to 3 Pv_{OXI} were sufficient to reach equilibrium. Leachate conductivity reached 3.5 mS/cm, 10.1 mS/cm, 10.2 mS/cm, and 15.2 mS/cm for oxidant concentrations of 2.6 g/L, 11.7 g/L, 12.9 g/L, and 19.5 g/L, respectively, in Col-Mn-1. In Col-Mn-2, leachate conductivity reached 3.6 mS/cm and 16.4 mS/cm for oxidant concentrations of 2.6 g/L and 19.8 g/L, respectively. The imposed conductivity (1500 mS/cm) was completely overrun by permanganate injection.

The redox potential (Eh) rose rapidly (after 1.5 Pv_{OXI} injected) from 318 ± 26 to 838 ± 18 mV with injection of the oxidant at 2.6 g/L and further to 900–920 mV at higher oxidant concentrations, showing saturation of the probe throughout the entire oxidation step.

The stop and flow time during oxidation did not induce noticeable variation of the water physicochemical parameters.

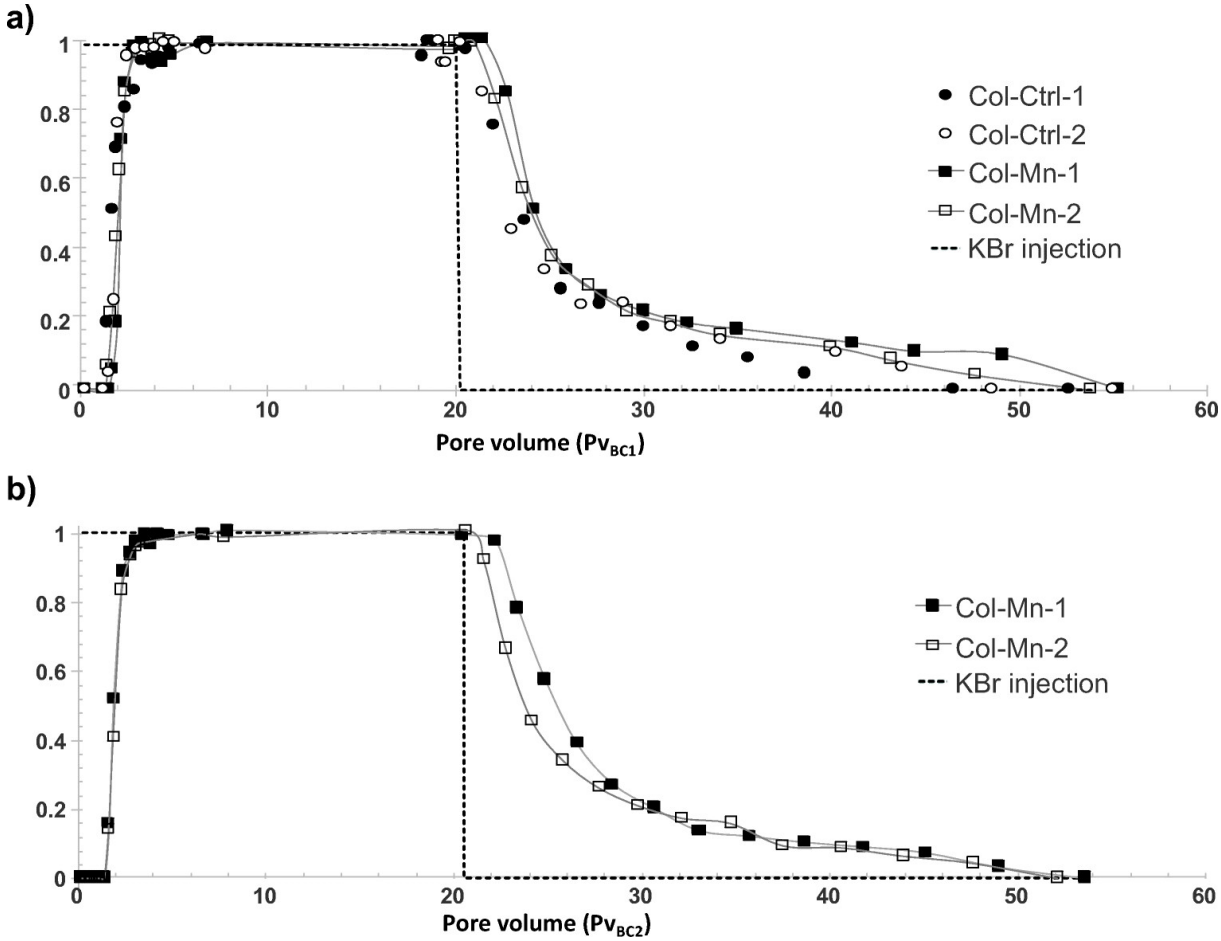

Fig. 3: Tracer experiment: a bromide ion breakthrough curves (BC1) measured for all replicates (Col-Ctrl-1 and Col-Ctrl-2 and Col-Mn-1 and Col-Mn-2) before oxidation; b bromide ion breakthrough curves (BC2) after oxidation and final water flushing (Col-Mn-1 and Col-Mn-2)

TOC concentration in the leachates The total organic carbon (TOC) concentration in the leachates decreased from 8.6 mg/L (end of sequence 2) to equilibrium at 2.8 mg/L after 20 Pv_{OXI} injection of $KMnO_4$ at a concentration of 2.6 g/L, whatever the column (Fig. 4). Higher concentrations of TOC were ob- served during stop-and-flow tests, with values depending on the stop duration. Higher TOC values were reach ed after the 69-h stop and flow (Pv_{OXI} = 38), with TOC concentrations of 16.4 and 11.6 mg/L for Col-Mn-1 and Col-Mn-2, respectively. For higher permanganate concentrations injected in continuous flushing, the TOC values decreased further to 1.0 mg/L.

UV absorbance/fluorescence fingerprints — evolution of permanganate in the outlet solution UV absorbance at 525 nm (permanganate) revealed that the permanganate concentrations in the water of the incoming and outcoming solutions were similar whatever the flow and the concentration, except in the case of the 69-h stop (a slight decrease of 0.36 g/L K MnO_4).

The fluorescent fingerprints (EEMs) of the water leachates during oxidation with permanganate were rapidly unusable (after Pv_{OXI} = 9), as the presence of the oxidant led to signal extinction.

Sequence 5: final water flushing (FWF)

Evolution of the physicochemical and spectroscopic water fingerprints The pH rapidly dropped to 7.0 and remained at this value for over 20 further Pv. Only the last two leachates (Pv_{FWF} = 80-83) exhibited a small pH increase up to 7.3.

After 19 Pv_{FWF} injection of WS, conductivity de- creased to 1600 µS/cm.

With final water flushing, the redox potential slowly decreased from 900 to 758 mV over the first 50 Pv_{FWF}, before a more rapid decrease down to 430 ± 4 mV with 22 more Pv_{FWF} for both columns.

For the first Pv_{FWF}, TOC values raised to 12.1 and 9.8 mg/L for Co l-Mn-1 and Col-Mn- 2, respectively. Then, these values decreased slowly over more than 50 Pv (from Pv_{FWF} = 12 to 74) to a minimum value of 1.8 ± 0.5 mg/L. Finally, the values roses lowly to 3.5 ± 0.4 mg/L with the last ten pore volumes, whatever the column.

Fluorescence spectrum measurements: the EEMs showed similar fingerprints throughout the sequence, without any visible difference with the HWF sequence fingerprints recorded before oxidation (Figure S3).

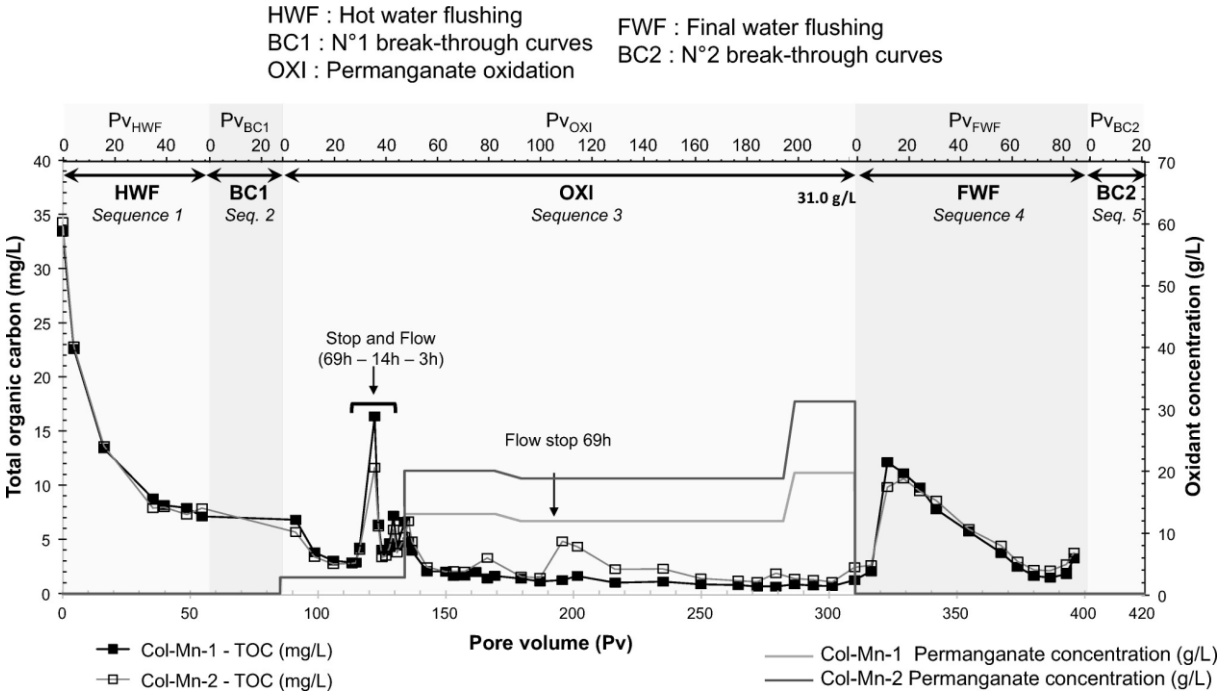

Fig. 4: Total organic carbon (TOC) values in the outcoming leachates from Col-Mn-1 and Col-Mn-2 from sequence 1 to 5 (hot water flushing (HWF), n°1 break-through curves (BC1), oxidation (OXY), final water flushing (FWF), and n°2 break-through curves (BC2)), overlapped with the oxidant concentrations applied in Col-Mn-1 and Col-Mn-2. The volumes eluted from the columns are given as total pore volumes (bottom X-axis) and as the pore volume (Pv) of each step (top X-axis)

Final breakthrough curves after oxidation (BC2)

Final breakthrough curves (sequence 6) were measured after final water flushing of the two columns (Col-Mn-1 and Col- Mn-2) at a constant flow rate (100 mL/h). The two replicates (Col-Mn-1 and Col-Mn-2) showed very similar evolutions of the bromide concentrations (Fig. 3b), with rapid ionic saturation of the porous medium (from Pv_{BC2} =1.6to Pv_{BC2} = 4.2). The ionic tracer concentration had a slightly longer desaturation step (over 3.5–5 pore volumes, from Pv_{BC2} =21.5 to Pv_{BC2} = 26.5). The start of desaturation slightly shifted (1.5 Pv) in Col-Mn-1 compared to Col-Mn-2 (Fig. 3b).

Column dismantling, DNAPL extraction, and analyses

GC-MS analyses, evolution of the PAH, and polar PAC proportions Changes in the molecular distribution of the DNAPL before (sequence 2 — hot water flushing) and after (sequence 6 — final water flushing) the oxidation step were determined by GC-MS analysis. Particles collected by filtering the outlet solution flushed out during oxidation were also analyzed. These particles included DNAPL blobs. Molecular proportions (PAHs and polar PACs) were calculated based on the peak area ratios from the GC-MS analyses (Table S3a & b). During permanganate treatment, the collected particles showed a lower HMW PAH/LMW PAH rato than the phases remaining in the columns, corresponding to 17–35% of the glass bead ratio. Only the particles collected at V_{FWF} =46 Pv gave a similar HMW PAH/LMW PAH ratio to the column DNAPL ratio.

EOM signatures in the column packing showed low depletion of O-PACs (furanes and ketones) after HWF and oxidation compared to the initial DN APL ratio (Fig. 5a, b, and c).

Particle/DNAPL blobs from permanganate treatment leachates exhibited a high enrichment in O-PAC ketones (Fig. 5d), especially in 9H-fluorenone (Table S3), compared to the EOM extracted from the columns before or after oxidation. This ratio remained high even after V_{FWF} =56 Pv eluted water (Fig. 5e). A thorough identification of the compounds detected in the eluted particles during oxidation (Pv_{OXI} =7,3 Pv) yielded a wide diversity of oxygenated compounds (mostly ketones and aldehydes) but also some alcohols and anhydrides. Main enrichment was observed for 9Hfluorenone (which represented 62.9% of the total quantified O-PACs), but other compounds were also enriched in relatively high proportions, e.g., anthraquinone and cyclopenta[*def*]phenanthrenone (3.4 % and 1.1 % of the total quantified OPACs, respectively).

Discussion

Repeatability of the experimental conditions

Initial DNAPL spiking: capillary pressure — saturation curves Overall, the four columns gave similar characteristics (glass bead mass, pore volume, measured residual water, and DNAPL saturation in the porous media — Table S2). The drainage-imbibition of the DNAPL in the porous medium resulted in irregular pollutant distribution in all columns (Figure S4), with DNAPL drops, pools, and some pores apparently free from organic phase. This organization corresponds to insular residual DNAPL saturation and is expected to be close to the field distribution of DNAPL in aquifers, following the displacement of the organic phase in contact with groundwater.

The drainage-imbibition curves showed a medium value of 10.9 ± 0.2 % vol residual DNAPL saturation in the porous medium. A mean curve was built using the data from the four replicates and was calibrated with the van Genuchten-Mualem (VGM) capillary pressure-saturation model (Mualem 1976; van Genuchten 1980) by the least squares method (Equation S1). Similar residual saturation (10.9 % ± 0.2) was calculated on the curve with the model, and the sums of squared errors (SSEs) were low (SSE<0.04 and SSE<0.10 for drainage and imbibition, respectively); this demonstrates that the experimental values agreed with the well-recognized VGM model. DNAPL residual saturation seemed consistent with dual systems (water-NAPL): residual saturation in sand can range from 15 to 50% of

the pore volume (Mercer and Cohen 1990), and soils exposed to coal tar can show residual saturation in column experiments between 7.7 and 22.6% depending on tar viscosity and soil composition (Kong 2004).

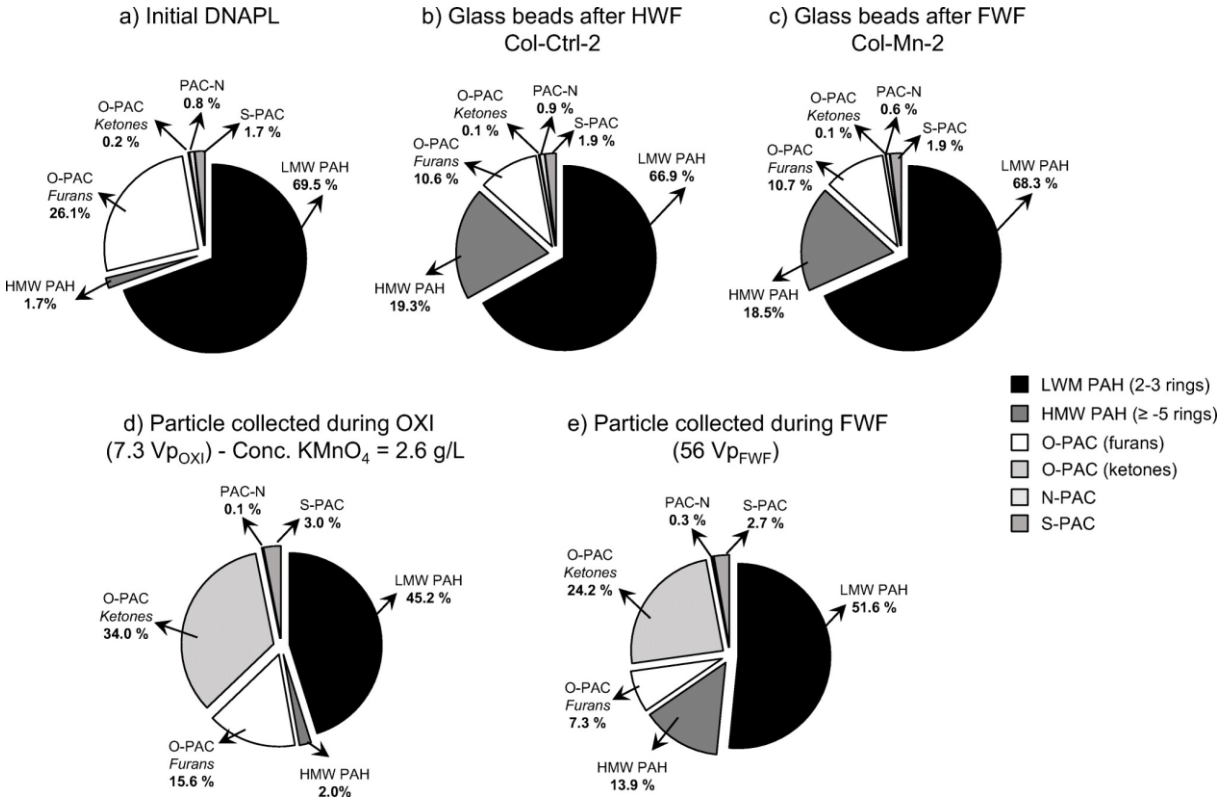

Fig. 5: Proportions of PAHs and polar PACs quantified by GC-MS in the total extractable organic matter from a the initial DNAP; b the glass beads after hot water flushing (HWF) in Col-Ctrl-2;c the glass beads after final water flushing (FWF) in Col-Ctrl-2 and from particles collected in the lixiviate of Col-Ctrl-2;d during permanganate injection (2.6 g/L) after injection of 7.3 pore volumes (Pv) of oxidant; and e after the final water flow injection of 56 Pv

The shape of the curves and the calculated VGM parameters (fitting parameter α =5.3 or 5.4m^{-1} and width of pore size distribution n = 5.7 or 6.8 for the drainage- imbibition curve, respectively) were consistent with those reported in other studies with glass beads and a dual water-air system of wetting and non-wetting fluid (Chiapponi 2017; Sweijen et al. 2017; Cao et al. 2018; Philippe et al. 2020). Moreover, the width of pore size distribution (parameter n) increased between drainage and imbibition, indicating that the heterogeneity of the porous medium was enhanced by the presence of residual DNAPL drops.

Only the DNAPL mass remaining in the whole system (column and cones) after the spiking step was more heterogeneous among columns.

Tracer experiment Before oxidation, the standard deviation of the bromide concentrations measured in each of the four columns was very low (0.036 ± 0.022), supporting a good hydraulic repeatability among replicates. This also reveals that the difference in the mass of DNAPL remaining in the entire system had no impact on hydraulic parameters.

The pore velocity calculated from the average retention time of the tracer (ascending curve) Pv = [1.7–2.0].10 −5 m/s was close to the water velocity of the aquifer measured near the source zone of our DNAPL ([7.3–11.5].10 −5 m/s).

Repeatability of the leachate parameters For all the following sequences, despite the differences in the amounts of residual DNAPL in the columns, each parameter analyzed in the leachate (pH, conductivity, TOC / TIC, UV, SUVA, etc.) showed similar results among the replicates.

Despite the two different flow rates applied during HWF (sequence 2), the leachate parameters at the end of this injection were similar in the four columns, attesting that (i) DNAPL acted as an infinite source and (ii) as far as pollutant drainage was concerned, the columns could be considered as replicates.

Fate of contaminants

Accuracy of the mass balance calculation and quantification of degradation efficiency The objective of this study was not to quantify oxidation efficiency accurately but to monitor the evolution of porosity and leachate quality. As mentioned in a previous study (Johansson et al. 2020), the high volatility of the studied DNAPL decreased the accuracy of the mass balance quantification. The purpose was to be close to field reality, hence the use of raw DNAPL with preserved volatile PACs.

The total lixiviated organic compounds were estimated for each column thanks to the periodic TOC measurements in the leachates. This cumulative mobilized TOC represented less than 0.5 wt% of the initial DNAPL mass. The organic compounds dissolved or remobilized by adsorption on particles did not represent a high proportion of the total pollutants inside the column.

Moreover, the evolution of UV absorbance at 525 nm revealed a limited consumption of $KMnO_4$ during the oxidative injections (data not shown). Therefore, it is likely that the degradation efficiency was extremely low.

Aging and stabilization of the pollutants The high total organic carbon content in the first water leachate (34.5 ± 1.9 mg/L) probably resulted from the dissolution equilibrium of all organic compounds from the DNAPL (one of the major organic compounds of the DNAPL was naphthalene, and its solubility in water is 32 mg/L at 25 °C), as the DNAPL and water were in contact for more than 2 weeks. With the beginning of the continuous injection, organic com- pounds did not reach this equilibrium, so that the TOC content decreased. The value stabilized after the elution of 50 Pv_{HWF} and probably corresponded to the dissolution equilibrium at this flow rate.

Higher flow rate injection slightly increased the TOC expelled from the columns, probably due to the higher temperature that caused higher dissolution of organic compounds. UV absorbance at 254 nm attested that the aromatic fingerprint increased rapidly in the outlet solutions during the two highest flushing rates. This increase can be explained by (i) an increase of the global PAC content or (ii) a preferential enrichment of higher molecular-weight aromatic compounds (more condensed rings) in the solution linked to the higher water temperature, as solubility increases with heat. The SUVA aromaticity index confirmed that the aromaticity of the mobilized organic compounds increased with the injection flow rate. The SUVA also showed a progressive increase throughout the total HWF step (sequence 2), probably due to gradual depletion of LMW PACs and a relative enrichment in HMW PACs.

At the beginning of the hot water flushing, LMW PACs (e.g., naphthalene, dibenzofuran) were probably in equilibrium with their solubility values (naphthalene and dibenzofuran solubilities are 32 mg/L and 5.3 mg/L, respectively), implying a predominance of these LMW PACs containing two aromatic rings. After the hot water injections, the dissolution equilibrium was modified. Slow depletion of LMW compounds from the DNAPL-water interfaces probably occurred and could ex- plain the final evolution of the leachate absorbance and the SUVA index despite the decreased TOC. The molecular GC- MS analyses of the remaining DNAPL after the HWF sequence (Col-Ctrl-1 and Col-Ctrl-2) seemed to confirm this hypothesis (Fig. 5). Many authors have shown that an interfacial high-viscosity skin-like film forms between water and tar pools with time (Alshafie and Ghoshal 2004; Luthy et al. 1993; Scherr et al. 2016). Relative enrichment in HMW structures at this interface has been measured (Ghoshal et al. 2004; Scherr et al. 2016), leading to a limited mass transfer of LMW compounds and more soluble

compounds from the DNAPL pool to the water phase (Alshafie and Ghoshal 2004; Ghoshal et al. 2004; Luthy et al. 1993; Scherr et al. 2016).

The global increase of the SUVA index and the decrease in TOC content during sequence 2 could be attributed to the progressive exhaustion of LMW PACs, probably due to the aging of the DNAPL-water interfaces. These changes limit the dissolution of pollutants, as already noticed in previous experiments by Boulangé et al. (2019a).

Impact of permanganate oxidation on DNAPL composition Permanganate is an oxidant known to be persistent in soils and groundwater, with oxidative activity over several months (Huling and Pivetz 2006; Simonnot and Croze 2012; Ranc et al. 2017). Its reaction is slow, especially on stable molecular organic structures; therefore, a loss of active oxidant flowing out of the column without being consumed was expected. However, even during the stop-and-flow steps (with stops of 3h, 14h, and 69h), oxidant consumption remained unexpectedly low, whereas batch oxidation had shown great activity of permanganate (> 80% of PAH degradation) after the first 3 h (Johansson et al. 2020). But higher proportions of oxidant were used (1 SOD) in that study, and the batches were shaken, inducing a constant renewal at the interfaces that favored the reaction.

When the oxidant was present (Fig. 4), the TOC content decreased in the water leachates, whereas higher concentrations of TOC were observed during the stop-and-flow events, depending on stop time duration (5.0 ± 2.1 and 4.4 ± 1.7 mg/L after 3h, 5.6 ± 1.0 and 4.8 ± 0.5 mg/L after 14h, and 16.4 and 11.6 mg/L after 69h for Col-Mn-1 and Col-Mn-2, respectively). This shows that both dissolution/transfer and degradation occurred in the column and may have driven the TOC concentrations in the water leachates depending on the imposed flow rate.

When the flow was stopped, the permanganate concentration in the pores was high enough to react with the organic molecules diffusing progressively from the DNAPL ganglions in solution. TIC measurements revealed carbonate accumulation consistent with total mineralization of organics (data not shown). When the reaction time was sufficient, the oxidant was largely consumed, and organic products accumulated in the pore water. According to Kim and Gurol (2005), degradation can become the limiting step when the concentration of oxidant decreases. Once the flow starts again, the organic compounds accumulated in water will be flushed, leading to an increased TOC content of the water leachates.

When the permanganate solution circulates, the oxidant is in excess. Our results show that it was poorly consumed due to the high flow rate (insufficient reaction time) and the low content in organic compounds in solution, hence limited diffusion. This limited diffusion can be controlled by the combination of the three following hypotheses:

1. The evolution of DNAPL composition at the interface with water, described above as aging (see the “Aging and stabilization of the pollutants” section)
2. The coating of MnO2 at the surface of DNAPL ganglions limiting the contact between oxidant and pollutants by reducing their dissolution and transfer (Conrad et al. 2002; Thomson et al. 2008; Petri et al. 2011)
3. The high ionic strength of the leachates due to an elevated amount of permanganate in solution, limiting dissolution of nonpolar molecules like PACs (Schwarzenbach et al. 2005; Mahjoub and Jayr 2000).

These results show that a high amount of DNAPL in the porous medium is poorly available for oxidation and questions the notion of an infinite source described above.

O-PAC formation A previous work (Johansson et al. 2020) highlighted that O-PACs were formed in high quantities during permanganate oxidation of DNAPL. They were still quantified after 7 days of oxidation in a batch experiment, while PAHs were nearly completely degraded. Therefore, their accumulation in the aqueous phase during the column experiments could be hypothesized.

The EOM molecular composition of the particles collected from the column during the treatment was marked by enrichment in ketones, especially 9H-fluorenone (which was also the main by-product observed in the batch experiments (Johansson et al. 2020)), compared to the composition of the DNAPL remaining in the column after oxidation (Fig. 5). This O-PAC enrichment probably came from PAH oxidation, and testified of an oxidative activity during permanganate injections.

Finally, 34.0 % of the total PACs quantified in the particles corresponded to furan-free O-PACs, whereas the remaining DNAPL in the column only contained 0.1 % of furan-free O-PACs. By comparison, other studies measured proportions of polar PACs ranging between 51 and 69% in the aqueous phase from coal tar leaching (Schlanges et al. 2008; Boulangé et al. 2019a). This could be explained by the preferential leaching of soluble O-PACs from the DNAPL ganglions. The collected particles also contained PAHs with a HMW PAH/LMW PAH ratio lower than those of the remaining DNAPL in the column after oxidation (Table S3a & b). LMW compounds are preferentially mobilized in the water column; as a consequence, they are more available for oxidation than HMW PAHs. The predominance of 9H-fluorenone compared to other O-PACs in the collected particles is consistent with partial oxidation of LMW PAHs by permanganate, as 9H-fluorenone is a by-product of the oxidation of fluorene, a LMW PAH.

In contrast, the aromatic compounds remaining in the column and identified by GC-MS did not show major differences in the ratios before and after oxidation (Table S3a). O-PACs were probably not produced in high enough quantities to impact the PAH/O-PAC ratio of the immobile remaining tar.

Impact of oxidation on the leachate signature after ending the permanganate injections A "bounce" of the TOC content was observed after ending oxidant injection (the flow was not stopped between oxidation and final water flushing). This increased TOC content was attributed to particle remobilization. During oxidation, MnO_2 particles are formed and are accumulated in the porous medium (Crimi and Siegrist 2004; Petri et al. 2011). With the decreased ionic strength at the beginning of the final water flow, charge repulsion of particles was enhanced, and MnO_2 dispersion in the water phase was favored (Boulangé et al. 2019a), leading to particle remobilization from the porous medium (Ryan and Gschwend 1994; Ryan and Elimelech 1996; VanNess et al. 2019).

Following this bouncing effect (Pv = 380), the pH started to rise slowly, and TOC stabilized at around 2.5 mg/L. The SUVA index of the last leachates (0.11 and 0.12 for ColMn-1 and Col-Mn-2, respectively) was similar to the SUVA index calculated at the end of hot water flushing (before oxidation). Moreover, the fluorescence fingerprints of the leachates before and after the oxidation step showed similar EEM spectra (Figure S3). No O-PAC–specific band (Hanser et al. 2015) was observed, suggesting that no or a too low proportion of O-PACs was mobilized compared to PAHs.

Once oxidation was stopped, and after the "bouncing" effect, the PAH composition of the leachates stabilized and seemed inherited form DNAPL dissolution, as already observed during the initial water flushing step (sequence 2). This observation is consistent with the limited degradation level of the DNAPL during the oxidation step.

Evolution of porosity

The breakthrough curves after final water flushing were similar to the one obtained before permanganate oxidation (Fig. 3), with an average standard deviation of 0.032 ± 0.032, in the same range as the standard deviation of all replicates before oxidation (0.036 ± 0.022) (Fig. 3). The slopes of the curves were also similar: the decreasing curve equations were $y=2.60\ e^{-1.09x}$ before oxidation and $y=2.63\ e^{-1.1x}$ after oxidation. The difference of the average values of C/C0 = 0.5, obtained at Pv = 23.96 before permanganate oxidation and Pv = 24.81 after final water flushing, corresponds to 3.42%. These results indicate that precipitated MnO_2 did not significantly reduce effective porosity and that the relative permeability of the water in the porous media is poorly influenced by oxidation.

Permanganate injections induced very little change in the hydraulic conductivity of the porous medium, in line with (i) the low quantity of precipitates formed due to low oxidative activity and (ii) the remobilization of those particles with the drop of ionic strength immediately after the end of oxidation. In contrast, many field studies have shown clogging of porous media during permanganate injections in soils (Heiderscheidt et al. 2008). The high hydraulic conductivity and homogeneity of our medium and its simplified composition (only glass beads without a nucleus to favor precipitation) may explain the difference between our results and field observations.

Conclusion

The aim of this study was to understand the impact of $KMnO_4$ under flow-through conditions and measure the consequences on hydraulic flow and water leachate quality.

Drainage (DNAPL injection) and imbibition (water injection) were used to spike the glass beads, resulting in an insular distribution of the pollutants with a nonhomogeneous distribution of drops and pools of pure organic phase, typical of the conditions encountered in soils after classical DNAPL pumping and treatment.

GC-MS analysis of the filtrated particles confirmed that as oxidation occurred, an increased O-PAC/PAH ratio was observed in the leachate. The results suggest that OPACs could be released during oxidation in an aquifer, as the chosen flow velocity was close to the one observed on site.

However, all the items of evidence suggest that permanganate oxidation was very limited, even if the oxidant dose was sufficient to mineralize about one third of the total DNAPL contained in the column. This result was unexpected in reference to literature data and because our experimental homogenous conditions were chosen to be representative of typical ISCO. It is explained by an aging process that prevents the DNAPL/water interface from being renewed and by the high ionic strength of the oxidant solution that slows down the dissolution of nonpolar aromatic structures. Oxidation is then limited to the dissolved and interfacial organic phases which are rapidly depleted with LMW PACs.

In field conditions, clogging and natural heterogeneities are known to limit the homogenous application of oxidants in an aquifer (preferential pathways). We also suggest that in situ oxidation by permanganate could be limited by interfacial aging of the DNAPL ganglions.

Acknowledgements

This work was supported by the French Environmental Agency (ADEME) and the French National Association for Research and Technology (ANRT). This work is included in the scientific program of the GISFI research consortium dedicated to knowledge and the development on remediation technologies for degraded and polluted lands (Groupement d'Intérêt Scientifique sur les Friches Industrielles — http://www.gisfi.univ-lorraine.fr). The authors thank the BRGM/DEPA division for its financial support. The authors are also grateful for the financial support provided to the PIVOTS project by the Centre-Val de Loire region (ARD 2020 program and CPER 2015-2020) and the French Ministry of Higher Education and Research (CPER 20152020 and public service subsidy to BRGM). They are also grateful to the European Union via the European Regional Development Fund for its support. We thank ArcelorMittal France for the assistance provided in the BIOXYVAL project, particularly for the provision of a site that allowed proper execution of the project work. We also thank Gilles Bessaque (GeoRessources) and Vincent Sauterau (BRGM) for their help in designing/constructing useful equipment. Petra Skacelova (NanoIron), Benjamin Douche (BRGM), and Audrey Dufour (CETRAHE) are thanked for their essential help during the experimentations and data treatment.

References

Alshafie M, Ghoshal S (2004) The role of interfacial films in the mass transfer of naphthalene from creosotes to water. J Contam Hydrol 74:283–298. https://doi.org/10.1016/j.jconhyd.2004.03.004

Andersson JT, Achten C (2015) Time to say goodbye to the 16 EPA PAHs? Toward an up-to-date use of PACs for environmental purposes. Polycycl Aromat Compd 35:330–354. https://doi.org/10.1080/10406638.2014.991042

Benhabib K, Faure P, Sardin M, Simonnot MO (2010) Characteristics of a solid coal tar sampled from a contaminated soil and of the organics transferred into water. Fuel 89:352–359. https://doi.org/10.1016/j. fuel.2009.06.009

Biache C, Ghislain T, Faure P, Mansuy-Huault L (2011) Low temperature oxidation of a coking plant soil organic matter and its major constituents: an experimental approach to simulate a long term evolution. J Hazard Mater 188:221–230. https://doi.org/10.1016/j. jhazmat.2011.01.102

Birak PS, Miller CT (2009) Dense non-aqueous phase liquids at former manufactured gas plants: challenges to modeling and remediation. J Contam Hydrol 105:81–98. https://doi.org/10.1016/j.jconhyd.2008. 12.001

Birdwell JE, Engel AS (2010) Characterization of dissolved organic matter in cave and spring waters using UV-Vis absorbance and fluorescence spectroscopy. Org Geochem 41:270–280. https://doi.org/10. 1016/j.orggeochem.2009.11.002

Boulangé M, Lorgeoux C, Biache C, Michel J, Michels R, Faure P (2019a) Aging as the main factor controlling PAH and polar-PAC (polycyclic aromatic compound) release mechanisms in historically coal-tar-contaminated soils. Environ Sci Pollut Res 26:1693–1705. https://doi.org/10.1007/s11356-018-3708-1

Boulangé M, Lorgeoux C, Biache C, Saada A, Faure P (2019b) Fenton like and potassium permanganate oxidations of PAH-contaminated soils: impact of oxidant doses on PAH and polar PAC (polycyclic aromatic compound) behavior. Chemosphere 224:437–444. https://doi.org/10.1016/j.chemosphere.2019.02.108

Broholm K, Jørgensen PR, Hansen AB, Arvin E, Hansen M (1999) Transport of creosote compounds in a large, intact, macroporous clayey till column. J Contam Hydrol 39:309–329. https://doi.org/10.1016/S0169-7722(99)00040-6

Brown DG, Gupta L, Kim TH, Keith Moo-Young H, Coleman AJ (2006) Comparative assessment of coal tars obtained from 10 former manufactured gas plant sites in the Eastern United States. Chemosphere 65:1562–1569. https://doi.org/10.1016/j. chemosphere.2006.03.068

Cao J, Jung J, Song X, Bate B (2018) On the soil water characteristic curves of poorly graded granular materials in aqueous polymer solutions. Acta Geotech 13:103–116. https://doi.org/10.1007/s11440017-0568-7

Chiapponi L (2017) Water retention curves of multicomponent mixtures of spherical particles. Powder Technol 320:646–655. https://doi.org/ 10.1016/j.powtec.2017.07.083

Chong AD, Mayer KU (2017) Unintentional contaminant transfer from groundwater to the vadose zone during source zone remediation of volatile organic compounds. J Contam Hydrol 204:1–10. https://doi. org/10.1016/j.jconhyd.2017.08.004

Coble P, Spencer R, Baker A, Reynolds D (2014) Aquatic organic matter fluorescence, Cambridge. Cambridge Univ Press, The Pitt Building, Trumpington St, Cambridge

Colombano S, Davarzani H, van Hullebusch ED, Huguenot D, Guyonnet D, Deparis J, Ignatiadis I (2020) Thermal and chemical enhanced recovery of heavy chlorinated organic compounds in saturated porous media: 1D cell drainage-imbibition experiments. Sci Total Environ 706:135758. https://doi.org/10.1016/j.scitotenv.2019. 135758

Conrad SH, Glass RJ, Peplinski WJ (2002) Bench-scale visualization of DNAPL remediation processes in analog heterogeneous aquifers: surfactant floods and in situ oxidation using permanganate. J Contam Hydrol 58:13–49. https://doi.org/10.1016/S0169-7722(02) 00024-4

Crimi ML, Siegrist RL (2004) Impact of reaction conditions on MnO2 genesis during permanganate oxidation. Journal of Environmental Engineering 130(5):562–572. https://doi.org/10.1061/(ASCE)07339372(2004)130:5(562)

Durant JL, Busby WF, Lafleur AL et al (1996) Human cell mutagenicity of oxygenated, nitrated and unsubstituted polycyclic aromatic hydrocarbons associated with urban aerosols. Mutat Res - Genet Toxicol 371:123–157. https://doi.org/10.1016/S0165-1218(96) 90103-2

Fellman JB, Hood E, Spencer RGM (2010) Fluorescence spectroscopy opens new windows into dissolved organic matter dynamics in freshwater ecosystems: a review. Limnol Oceanogr 55:2452–2462. https://doi.org/10.4319/lo.2010.55.6.2452

Ferretto N, Tedetti M, Guigue C, Mounier S, Redon R, Goutx M (2014) Identification and quantification of known polycyclic aromatic hydrocarbons and pesticides in complex mixtures using fluorescence excitation-emission matrices and parallel factor analysis. Chemosphere 107:344–353. https://doi.org/10.1016/j. chemosphere.2013.12.087

Forsey SP, Thomson NR, Barker JF (2010) Oxidation kinetics of polycyclic aromatic hydrocarbons by permanganate. Chemosphere 79: 628–636. https://doi.org/10.1016/j.chemosphere.2010.02.027

Ghoshal S, Pasion C, Alshafie M (2004) Reduction of benzene and naphthalene mass transfer from crude oils by aging-induced interfacial films. Environ Sci Technol 38:2102–2110. https://doi.org/10.1021/es034832j

Guan W, Xie Z, Zhang J (2014) Preparation and aromatic hydrocarbon removal performance of potassium ferrate. J Spectrosc, ID 171484 8 pages 2014:1–8. https://doi.org/10.1155/2014/171484

Hanser O, Biache C, Boulangé M, Parant S, Lorgeoux C, Billet D, Michels R, Faure P (2015) Evolution of dissolved organic matter during abiotic oxidation of coal tar - comparison with contaminated soils under natural attenuation. Environ Sci Pollut Res 22:1431– 1443. https://doi.org/10.1007/s11356-014-3465-8

He D, Guan X, Ma J, Yang X, Cui C (2010) Influence of humic acids of different origins on oxidation of phenol and chlorophenols by permanganate. J Hazard Mater 182:681–688. https://doi.org/10.1016/j. jhazmat.2010.06.086

Heiderscheidt JL, Crimi M, Siegrist RL, Singletary MA (2008) Optimization of full-scale permanganate ISCO system operation: laboratory and numerical studies. Ground Water Monitoring and Remediation 28(4):72–84. https://doi.org/10.1111/j.1745-6592. 2008.00213.x

Huling, S.G. and Pivetz, B.E. 2006. In-situ chemical oxidation, Cincinnati, Ohio: United States Environmental Protection Agency. EPA/600/R-06/072

Jeanneau L, Faure P, Jarde E (2007) Influence of natural organic matter on the solid phase extraction of lipids. Application to particulate, colloidal and truly dissolved fractions of the water-extract from highly contaminated river sediment. Journal of Chromatographia A 1173:1–9. https://doi.org/10.1016/j.chroma.2007.09.080

Johansson C, Bataillard P, Biache C, Lorgeoux C, Colombano S, Joubert A, Pigot T, Faure P (2020) Ferrate VI oxidation of polycyclic aromatic compounds (PAHs and polar PACs) on DNAPL-spiked sand: degradation efficiency and oxygenated by-product formation compared to conventional oxidants. Environ Sci Pollut Res 27:704–716. https://doi.org/10.1007/s11356-019-06841-0

Kim K, Gurol MD (2005) Reaction of nonaqueous phase TCE with permanganate. Environ Sci Technol 39:9303–9308. https://doi.org/ 10.1021/es050830i

Kleineidam S, Rügner H, Grathwohl P (2004) Desorption kinetics of phenanthrene in aquifer material lacks hysteresis. Environ Sci Technol 38:4169–4175. https://doi.org/10.1021/es034846p

Kong L (2004) Characterization of mineral oil, coal tar and soil properties and investigation of mechanisms that affect coal tar entrapment in and removal from porous media. PhD thesis, School of Civil and Environmental Engineering, Georgia Institute of Technology, Atlanta, GA, 309p

Lampi MA, Gurska J, McDonald KIC et al (2006) Photoinduced toxicity of polycyclic aromatic hydrocarbons to Daphnia magna: ultraviolet mediated effects and the toxicity of polycyclic aromatic hydrocarbon photoproducts. Environ Toxicol Chem 25:1079–1087. https:// doi.org/10.1897/05-276R.1

Lemaire J, Buès M, Kabeche T et al (2013a) Oxidant selection to treat an aged PAH contaminated soil by in situ chemical oxidation. J Environ Chem Eng 1:1261–1268. https://doi.org/10.1016/j.jece.2013.09.018

Lemaire J, Laurent F, Leyval C, Schwartz C, Buès M, Simonnot MO (2013b) PAH oxidation in aged and spiked soils investigated by column experiments. Chemosphere 91:406–414. https://doi.org/10.1016/j.chemosphere.2012.12.003

Lemaire J, Mora V, Faure P, Hanna K, Buès M, Simonnot MO (2019) Chemical oxidation efficiency for aged, PAH-contaminated sites: An investigation of limiting factors. J Environ Chem Eng 7: 103061. https://doi.org/10.1016/j.jece.2019.103061

Lundstedt S, White PA, Lemieux CL, Lynes KD, Lambert IB, Öberg L, Haglund P, Tysklind M (2007) Sources, fate, and toxic hazards of oxygenated polycyclic aromatic hydrocarbons (PAHs) at PAH contaminated sites. Ambio 36:475–485. https://doi.org/10.1579/ 0044-7447(2007)36[475:sfatho]2.0.co;2

Luthy RG, Ramaswami A, Ghoshal S, Merkel W (1993) Interfacial films in coal tar nonaqueous-phase liquid-water systems. Environ Sci Technol 27:2914–2918. https://doi.org/10.1021/es00049a035

Mahjoub B, Jayr E (2000) Phase partition of organic pollutants between coal tar and water under variable experimental conditions. Water Research 34:3551–3560. https://doi.org/10.1016/S0043-1354(00) 00100-7

Matta R, Chiron S (2018) Oxidative degradation of pentachlorophenol by permanganate for ISCO application. Environ Technol (United Kingdom) 39:651–657. https://doi.org/10.1080/09593330.2017.1309077

Mercer JW, Cohen RM (1990) A review of immiscible fluids in the subsurface: properties, models, characterization and remediation. J Contam Hydrol 6:107–163. https://doi.org/10.1016/0169-7722(90) 90043-G

Mualem Y (1976) A new model for predicting the hydraulic conductivity of unsaturated porous media. Water Resour Res 12:513–522. https:// doi.org/10.1029/WR012i003p00513

Pardo F, Santos A, Romero A (2016) Fate of iron and polycyclic aromatic hydrocarbons during the remediation of a contaminated soil using iron-activated persulfate: a column study. Sci Total Environ 566– 567:480–488. https://doi.org/10.1016/j.scitotenv.2016.04.197

Parlanti E, Wörz K, Geoffroy L, Lamotte M (2000) Dissolved organic matter fluorescence spectroscopy as a tool to estimate biological activity in a coastal zone submitted to anthropogenic inputs. Org Geochem 31:1765–1781. https://doi.org/10.1016/S0146-6380(00)00124-8

Pedersen DU, Durant JL, Penman BW, Crespi CL, Hemond HF, Lafleur AL, Cass GR (2004) Human-cell mutagens in respirable airborne particles in the Northeastern United States. 1. Mutagenicity of Fractionated Samples. Environ Sci Technol 38:682–689. https:// doi.org/10.1021/es0347282

Petri BG, Thomson NR, Urynowicz MA (2011) Fundamentals of ISCO using permanganate. In: Siegrist RL, Crimi M, Simpkin TJ (eds) In Situ Chemical Oxidation for Groundwater Remediation. pp 89–138

Philippe N, Davarzani H, Marcoux M, Colombano S, Dierick M, Klein PY (2020) Experimental study of the temperature effect on two phase flow properties in highly permeable porous media:

application to the remediation of dense non-aqueous phase liquids (DNAPLs) in polluted soil. Advances in Water Resources 146:103783. https://doi. org/10.1016/j.advwatres.2020.103783

Ranc B, Faure P, Croze V, Simonnot MO (2016) Selection of oxidant doses for in situ chemical oxidation of soils contaminated by polycyclic aromatic hydrocarbons (PAHs): a review. J Hazard Mater 312:280–297. https://doi.org/10.1016/j.jhazmat.2016.03.068

Ranc B, Faure P, Croze V, Lorgeoux C, Simonnot MO (2017) Comparison of the effectiveness of soil heating prior or during in situ chemical oxidation (ISCO) of aged PAH-contaminated soils. Environ Sci Pollut Res 24:11265–11278. https://doi.org/10.1007/ s11356-017-8731-0

Ryan JN, Elimelech M (1996) Colloid mobilization and transport in groundwater. Colloids Surfaces A Physicochem Eng Asp 107:1–56

Ryan JN, Gschwend PM (1994) Effects of ionic strength and flow rate on colloid release: relating kinetics to intersurface potential energy. J. Colloid Interface Sci. 164:21–34. https://doi.org/10.1006/jcis.1994. 1139

Scherr KE, Vasilieva V, Lantschbauer W, Nahold M (2016) Composition and dissolution of a migratory, weathered coal tar creosote DNAPL. Front Environ Sci 4:1–10. https://doi.org/10.3389/fenvs.2016. 00061

Schlanges I, Meyer D, Palm W-U, Ruck W (2008) Identification, quantification and distribution of Pac-metabolites, heterocyclic Pac and substituted Pac in groundwater samples of tar-contaminated sites From Germany. Polycycl Aromat Compd 28:320–338. https://doi. org/10.1080/10406630802377807

Schwarzenbach R, Gschwend P, Imboden D (2005) Environmental organic chemistry, Second Edition

Simonnot M-O, Croze V (2012) Traitement des sols et nappes par oxydation chimique in situ. Technique de l'Ingénieur - Génie des Procédés et protection de l'environnement, J3983

Sirguey C, Tereza de Souza e Silva P, Schwartz C, Simonnot MO (2008) Impact of chemical oxidation on soil quality. Chemosphere 72:282– 289. https://doi.org/10.1016/j.chemosphere.2008.01.027

Sverdrup LE, Ekelund F, Krogh PH, Nielsen T, Johnsen K (2002) Soil microbial toxicity of eight polycyclic aromatic compounds: effects on nitrification, the genetic diversity of bacteria, and the total number of protozoans. Environ Toxicol Chem 21:1644–1650. https:// doi.org/10.1002/etc.5620210815

Sweijen T, Aslannejad H, Hassanizadeh SM (2017) Capillary pressure– saturation relationships for porous granular materials: pore morphology method vs. pore unit assembly method. Adv Water Resour 107: 22–31. https://doi.org/10.1016/j.advwatres.2017.06.001

Tedetti M, Guigue C, Goutx M (2010) Utilization of a submersible UV fluorometer for monitoring anthropogenic inputs in the Mediterranean coastal waters. Mar Pollut Bull 60:350–362. https:// doi.org/10.1016/j.marpolbul.2009.10.018

Thomson NR, Fraser MJ, Lamarche C, Barker JF, Forsey SP (2008) Rebound of a coal tar creosote plume following partial source zone treatment with permanganate. J Contam Hydrol 102:154–171. https://doi.org/10.1016/j.jconhyd.2008.07.001

Touraud E, Crone M, Thomas O (1998) Rapid diagnosis of polycyclic aromatic hydrocarbons (PAH) in contaminated soils with the use of ultraviolet detection. In: Field Analytical Chemistry and Technology 2:221–229

Trellu C, Mousset E, Pechaud Y, Huguenot D, van Hullebusch ED, Esposito G, Oturan MA (2016) Removal of hydrophobic organic pollutants from soil washing/flushing solutions: a critical review. J Hazard Mater 306:149–174. https://doi.org/10.1016/j.jhazmat.2015. 12.008

Usman M, Faure P, Lorgeoux C, Ruby C, Hanna K (2013) Treatment of hydrocarbon contamination under flow through conditions by using magnetite catalyzed chemical oxidation. Environ Sci Pollut Res 20: 22–30. https://doi.org/10.1007/s11356-012-1016-8

Usman M, Hanna K, Haderlein S (2016) Fenton oxidation to remediate PAHs in contaminated soils: a critical review of major limitations and counter-strategies. Sci Total Environ 569:179–190. https://doi. org/10.1016/j.scitotenv.2016.06.135

van Genuchten M (1980) A closed-form equation for predicting the hydraulic conductivity of unsaturated soils. Soil Sci Soc Am J 44:892– 898

VanNess K, Rasmuson A, Ron CA, Johnson WP (2019) A unified force and torque balance for colloid transport: predicting attachment and mobilization under favorable and unfavorable conditions. Langmuir 35:9061–9070. https://doi.org/10.1021/acs.langmuir.9b00911

Venny GS, Ng HK (2012) Inorganic chelated modified-Fenton treatment of polycyclic aromatic hydrocarbon (PAH)-contaminated soils. Chem Eng J 180:1–8. https://doi.org/10.1016/j.cej.2011.10.082

Waldemer R, Tratnyek PG (2006) Kinetics of contaminant degradation by permanganate. Environ Sci Technol 40:1055–1061. https://doi. org/10.1021/es051330s

Wehrer M, Totsche KU (2005) Determination of effective release rates of polycyclic aromatic hydrocarbons and dissolved organic carbon by column outflow experiments. Eur J Soil Sci 56:803–813. https://doi. org/10.1111/j.1365-2389.2005.00716.x

Xue W, Warshawsky D (2005) Metabolic activation of polycyclic and heterocyclic aromatic hydrocarbons and DNA damage: a review. Toxicol. Appl. Pharmacol. 206:73–93. https://doi.org/10.1016/j. taap.2004.11.006

Supplementary materials

C. Johansson, P. Bataillard, C. Biache, C. Lorgeoux, S. Colombano, A. Joubert, C. Défarge, P. Faure

Permanganate oxidation of Polycyclic Aromatic Compounds (PAHs and polar PACs): 1D-column experiments with DNAPL at residual saturation

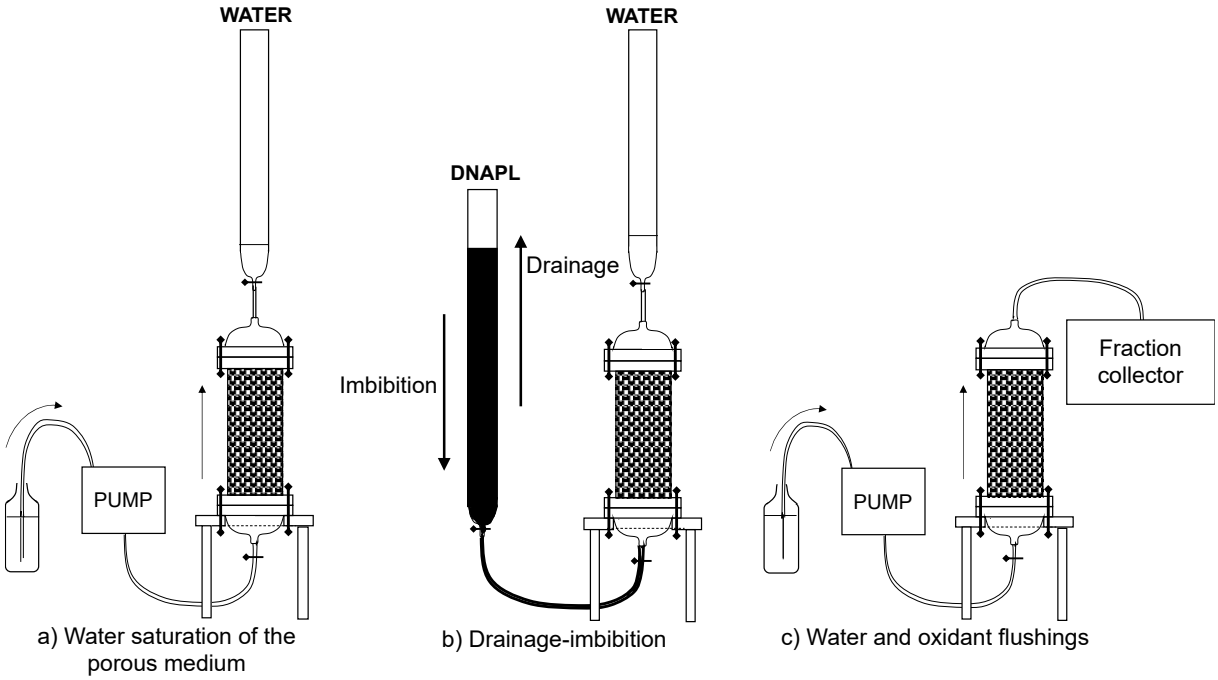

Figure S1: Diagram of a) water saturation of the porous medium; b) drainage – imbibition; and c) water and oxidation flushing steps.

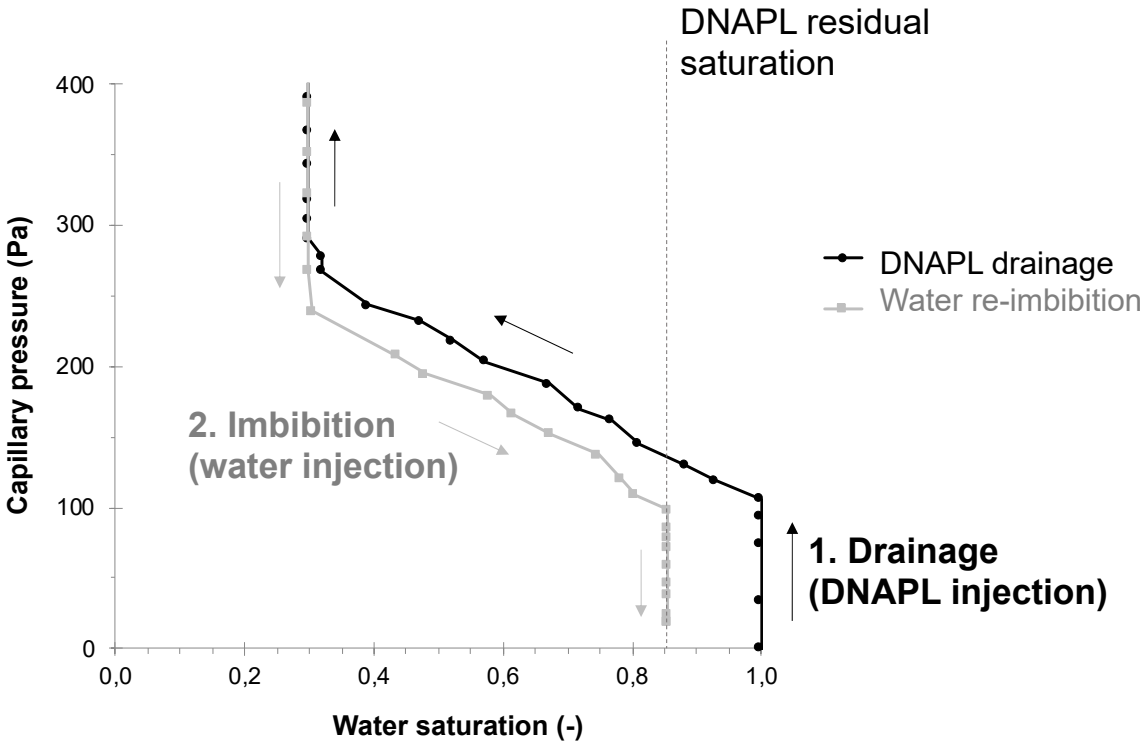

Figure S2: Drainage - imbibition curves for Col-Mn-2: (1) DNAPL drainage curve; (2) water imbibition curve in the glass beads (1 mm). Similar curves were obtained for all replicates (Col-Ctrl-1 & -2, Col-Mn-1).

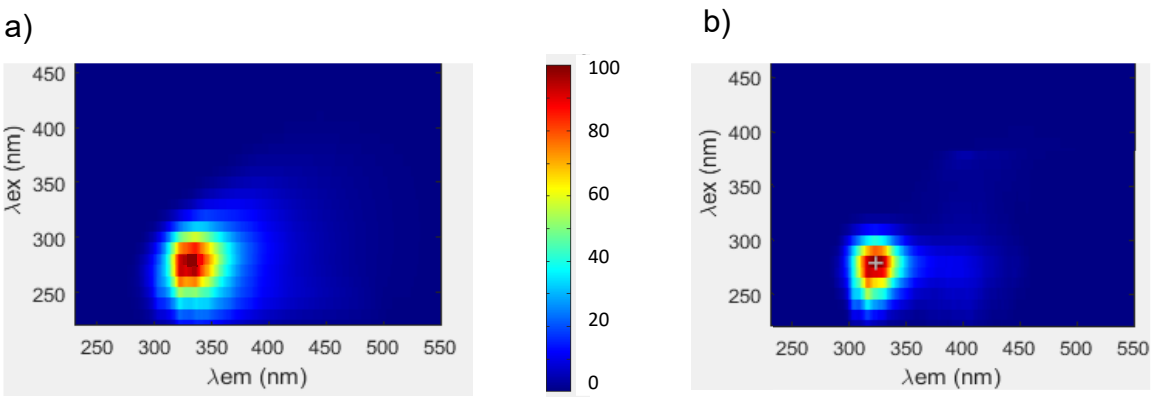

Figure S3: Emission-excitation matrices of the lixiviate at the end of (a) hot water flushing (HWF) and (b) final water flushing (FWF).

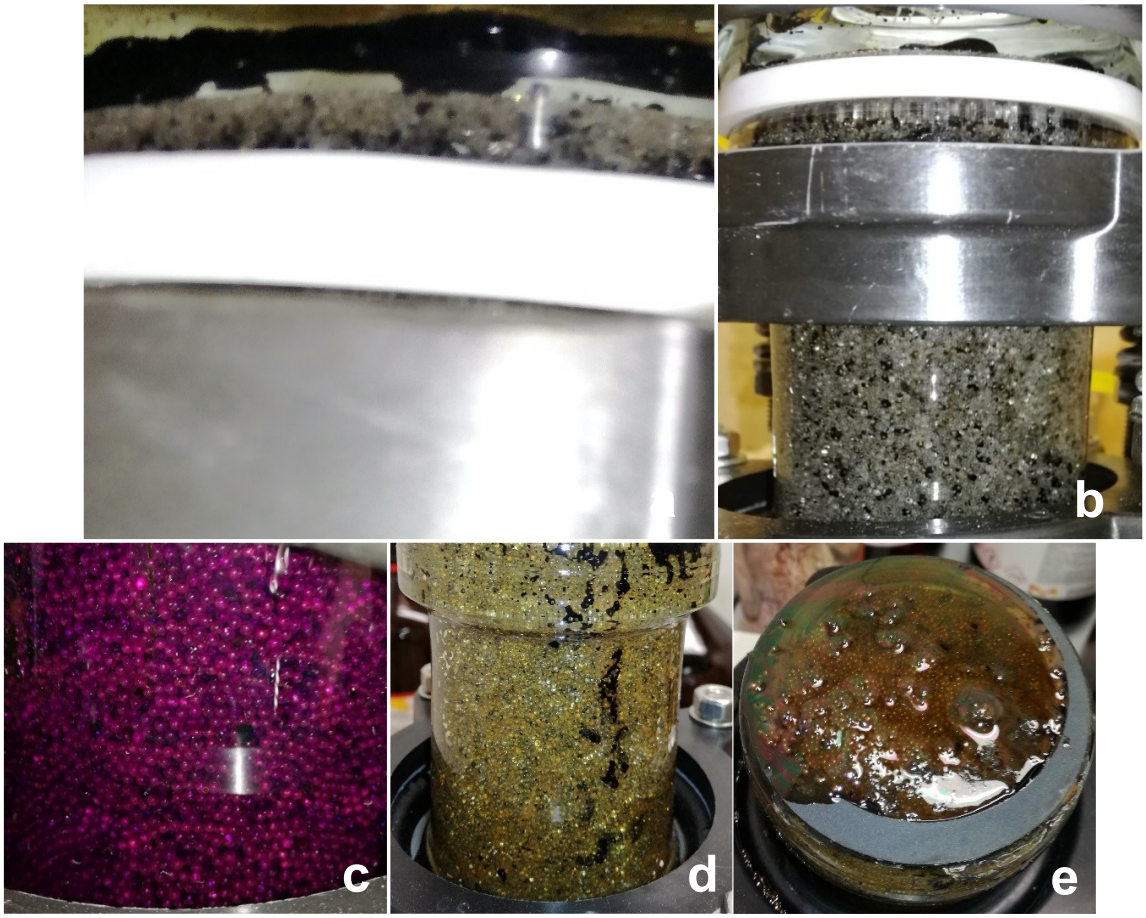

Figure S4: Photographs of the Col-Mn-1 glass bead column (a) after drainage – imbibition; (b) during hot water flushing; (c) during permanganate injection at a concentration of 2,6 g/L; (d) after the end of the oxidation sequence; and (e) after final water flushing.

Equation S1 - Van Genuchten Mualem model

$$S_{ew} = \frac{1}{[1 + (\alpha h_c)^n]^m}$$

$$S_{ew} = \frac{S_w - S_{rw}}{1 - S_{rw}}$$

$$S_w = S_{ew}(1 - S_{rw} - S_{rn}) + S_{rw}$$

with:
S_{ew}: effective saturation (-)
S_w: water (wetting fluid) saturation
S_{rw}: water (wetting fluid) residual saturation
S_{rn}: DNAL (non-wetting fluid) residual saturation
h_c: capillary head (m)
α: fitting parameter inversely proportional to the non-wetting fluid entry pressure value (m^{-1})
n: width of pore size distribution (-)
m=1-1/n

Table S1 - (m/z) value of each PAC used for the single ion monitoring GC-MS analyses

PAHs (m/z)	
Naphthalene D8	136
Naphthalene	128
Acenaphthylene	152
Acenaphthene D10	164
Acenaphthene	153
Fluorene	166
Phenanthrene D10	188
Phenanthrene	178
Anthracene	178
Fluoranthene	202
Pyrene D10	212
Pyrene	202
Benz[*a*]anthracene	228
Chrysene D12	240
Chrysene	228
Benzo[*b*]fluoranthene	252
Benzo[*k*]fluoranthene	252
Benz[*a*]pyrene	252
Perylene D12	264
Perylene	252
Indeno[1,2,3-*cd*]pyrene	276
Dibenz[*a,h*]anthracene	278
Benzo[*ghi*]perylene	276

Oxygenated PACs (m/z)	
Dibenzofuran	168
4-methyldibenzofuran	181
9H-fluorenone D8	188
9H-fluorenone	180
Perinaphtenone	152
Anthraquinone	208
Cyclopenta[*def*]phenanthrone	204
Methylanthracene-9,10-dione	165
Benz[*a*]fluorenone	230
Benzanthrone	230
Benzoanthracenedione	258
Naphtacene-5,12-dione	258
Benzo[*cd*]pyrenone	254

Nitrogenated PACs (m/z)	
Quinoline D7	136
Quinoline	129
Benzo[*h*]quinoline	179
Acridine	179
Carbazole	167
Benzo[a]carbazole	217
Benzo[*c*]acridine	229
Nitropyrene	201

Sulphur-containing PAC (m/z)	
Benzothiophene	134
2-methylbenzo[*b*]thiophene	147
Dibenzothiophene	184
4-methyldibenzothiophene	198

Table S2 - Glass bead mass, pore volume and residual water and DNAPL saturations deduced from the drainage-imbibition curves and the mass of total remaining DNAPL for each column.

Glass beads	Col-Ctrl-1	Col-Ctrl-2	Col-Mn-1	Col-Mn-2	Mean value
Mass of glass beads (g)	340.7	335.4	332.6	336.4	336.3 ± 3.4
Pore volume (PV) (mL)	71.9	68.8	70.6	72.6	71.0 ± 1.7
Porosity (%)	0.40	0.38	0.39	0.40	0.39 ± 0.1
Residual water saturation after drainage (% volume) in PV	**27.7**	**35.3**	**29.1**	**29.8**	**30.5 ± 3.3**
DNAPL in pore volume (mL)	*44.2*	*33.5*	*41.5*	*42.8*	*40.5 ± 4.8*
Calculated mass of DNAPL (d=1.09) in PV after drainage (g)	*40.5*	*30.8*	*38.0*	*39.2*	*37.1 ± 4.3*
Residual DNAPL saturation after imbibition (% vol.) in PV	**8.8**	**8.8**	**9.0**	**8.6**	**8.8 ± 0.2**
DNAPL in pore volume (mL)	6.3	6.1	6.3	6.2	6.2 ± 0.1
Calculated mass of DNAPL (d=1.09) in PV after imbibition (g)	6.9	6.6	6.9	6.8	6.8 ± 0.1
DNAPL mass weighed in the whole system (column, cones, tubes) (g)	**20.2**	**21.4**	**27.4**	**42.6**	**27.9 ± 10.3**

Table S3 - Ratios of PAH and O-PAC abundance (GC-MS quantification) obtained from a) extracted glass beads after the treatments; and b) extracted particles collected from the leachates on the filters during the treatments (PV = pore volume).

a) Glass beads	**Glass beads** ***Average value after hot water flushing***	**Glass beads** ***Average value after $KMnO_4$ oxidation***
HMW PAHs / LMW PAHs*	0.2 + 0.0 95 /- 11	0.2 + 0.0 70 /- 02
9H-fluorenone/ fluorene	0.0 + 0.0 03 /- 01	0.0 + 0.0 05 /- 01
10 ketone O-PACs / PAHs	0.0 + 0.0 01 /- 001	0.0 + 0.0 01 /- 001

	Filters collected during permanganate injections on Col-Mn-1				
b) Leachate particles	**(PV_{Ox}= 7.5) 2.6 g/L**	**(PV_{Ox}= 164-171) 11..67 g/L**	**(PV_{Ox}= 164-171) 18.6 g/L**	**(PV_{FWF}= 46) 0 g/L**	**(PV_{FWF}= 56) 0 g/L**
HMW PAHs / LMW PAHs*	0.045	0.095	0.095	0.269	0.067
9H-fluorenone / fluorene	168.4	118.1	228.7	265.8	307.6
10 ketone O-PACs / PAHs	0.72	0.62	0.41	0.37	0.53

** low-molecular-weight (LMW) PAHs = 2-3-ring PAHs; high-molecular-weight (HMW) PAHs = 4-ring PAHs.*